Vilniaus Universitetas
Fizikos Fakuletas
Kvantinės Elektronikos Katedra

Agneška Šablovskaja

MARSO ORGANINIŲ MOLEKULIŲ ANALIZATORIUI SKIRTOS SKAIDRINANČIOS DANGOS TYRIMAS, STEBINT LAZERINE SPINDULIUOTE SUKELTĄ TARŠĄ

Magistrantūros studijų baigiamasis darbas

Lazerinės technologijos studijų programa

Studentė	Agneška Šablovskaja
Darbo vadovas	doc. dr. Andrius Melninkaitis
Konsultantas	dr. rer. nat. Matthias Ließmann
Recenzentas	dr. Rytis Buzelis
Katedros vedėjas	prof. habil. dr. Valdas Sirutkaitis

Vilnius 2016

Vilnius University
Faculty of Physics
Department of Quantum Electronics

Agneška Šablovskaja

LASER-INDUCED CONTAMINATION ON ANTI-REFLECTIVE COATING USED IN MARS ORGANIC MOLECULE ANALYSER

Master thesis

Laser technology study program

Student	Agneška Šablovskaja
Supervisor	doc. dr. Andrius Melninkaitis
Consultant	dr. rer. nat. Matthias Ließmann
Reviewer	dr. Rytis Buzelis
Head of department	prof. habil. dr. Valdas Sirutkaitis

Vilnius 2016

Acknowledgements

This Thesis is part of the „ExoMars rover 2018“ ESA led project. The development of laser-system that will be installed in ExoMars rover and the qualification of used optical components and materials regarding LIC are entrusted to The Laser Zentrum Hannover e.V.

Research project was performed at the Laser Zentrum Hannover e.V., Germany.

This work is funded by the German Aerospace Centre (DLR), grant no. 50QX1002 and 50QX1402. The development was and is carried out in close cooperation with the Max Planck Institute for Solar System Research and the Goddard Space Flight Centre.

Thanks to supervisor dr. rer. nat. Matthias Ließmann, Head of Characterization Group Dr.rer.nat. Lars Jensen and Laser Development Department.

Table of Contents

Glossary

Symbol	Explanation
ALADIN	Atmospheric Laser Doppler Instrument
AR	Anti-Reflective
CCD	Charge-Coupled Device
CMOS	Complementary Metal Oxide Silicon
CVCM	Collected Volatile Condensable Material
DIC	Differential Interference Contrast
e-Beam	Electron Beam Evaporation
ESA	European Space Agency
HR	High-Reflective
IAD	Ion Assisted Deposition
IBS	Ion Beam Sputtering
ITMS	Ion Trap Mass Spectrometer
LDI	Laser Desorption Ionization
LIC	Laser-Induced Contamination
LIDT	Laser-Induced Damage Threshold
LIF	Laser-Induced Fluorescence
$LiNbO_3$	Lithium Niobate
LZH	Laser Centre in Hanover (Laser Zentrum Hannover)
MS	Magnetron Sputtering
MOMA	Mars Organic Molecule Analyser
NBOHC	Non-Bridging Oxygen Hole Centres
Nd:YAG	Neodymium-Doped Yttrium Aluminium Garnet
ODC	Oxygen Deficient Centres
pyr-GC	pyrolysis-Gas Chromatography
POR	Peroxy Radicals
PVD	Physical vapour Deposition
STE	Self-Trapped Excitons
STH	Self-Trapped Holes
TML	Total Mass Loss
UV	Ultraviolet
UHV	Ultra-High Vacuum
WVR	Water Vapour Regained

α	Angle of Incidence
λ	Wavelength
τ	Pulse duration
D_{eff}	Beam Diameter in the Target Plane
D	Diameter
E_{p}	Pulse energy
E	Electric field
h	Thickness
H	Fluence
$F_{i,k}$	Force
f_{p}	Pulse Repetition Rate
g	Gravity
n	Refractive index
P	Polarization
r	Radius
t	Transmittance
T	Temperature

Introduction

Evolving technologies allow new discoveries on the earth as well as in space. New ExoMars rover mission led by ESA will launch on 2018 with the aim of seeking for the manifestations of life. For molecular compound characterization ExoMars rover contains Mars Organic Molecule Analyser (MOMA). Data collected by MOMA should give answers to questions related to the origin, evolution and distribution of Martian life forms [1]. MOMA is a complex instrument with a number of components, including ion trap mass spectrometer (ITMS). The ITMS supports pyrolysis-gas chromatography (pyr-GC) as well as Laser Desorption Ionization (LDI) analyses. LDI refers to triggering of sample surface ablation and desorption by laser beam and the ionization of analyte molecules in the plasma plume above the ablated surface. For efficient desorption of the sample from soil of Mars and its ionization, nanosecond-pulsed frequency-quadrupled (266 nm) passively Q-switched Nd:YAG laser with the energy of laser pulse up to 200 micro Joules (μJ) and the intensities of tens to hundreds of Mega Watts in squared centimetre (MW/cm^2) is used [2, 3].

Development of high-power laser systems for space applications is not straightforward task as various harmful changes on optics can be induced by space environment. Analysis of previously failed space missions showed that the lifetime of ultraviolet laser optics in space is lowered due to the vacuum impact on material outgassing rates and laser-induced contamination (LIC). LIC refers to deposit build-up on optical sample that is irradiated by laser beam. Even though by now there is quite a lot information on LIC in UV range (355 nm), measurements with 266 nm just has been started few months ago and results indicate that LIC is even more severe in case of 266 nm irradiation under conditions that were chosen for first tests [4]. But there is no enough of data to draw conclusions about general behaviour of laser-induced contamination growth under 266 nm irradiation as LIC has been shown to be critical in some cases and in other cases not. This brings the necessity to test the effect of every possible MOMA laser system contamination source under working conditions on optics.

Accordingly, the main goal of this research is to estimate behaviour of Laser-Induced Contamination growth on AR coatings used in Mars Organic Molecule Analyser.

Research tasks:

1) To assemble test bench for LIC measurements at 266 nm wavelength;
2) Optimize and characterize the LIC test bench;
3) To observe laser-induced contamination build-up on AR coated fused silica caused by different outgassing materials used in MOMA laser;
4) To analyse the rates of contamination build-up and confirm whether material is compatible for this application or not.

1. Literature overview

1.1 Space environment effects on optical components

Optical components used in spacecraft might have to operate under conditions that differ from the ones on the Earth. These conditions vary depending on the mission. The main space environment effects that might induce changes in spaceborne optics are shown in Fig. 1. There are other effects like rapid temperature changes, cryogenic temperatures or very high temperature, vibrational loads during lift off and landing, different strength of gravitational fields and so on [5].

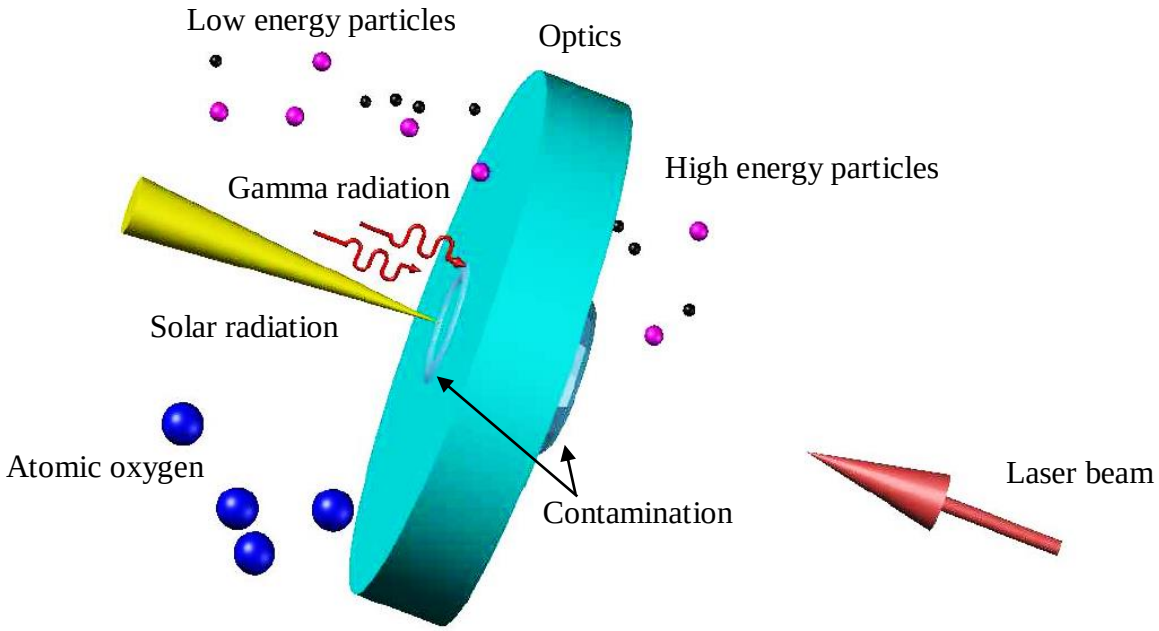

Figure 1. Representative drawing of main space environment effects that might induce changes in spaceborne optics.

Space environmental conditions that are mentioned above might cause different changes in optical components:

- The reduced laser-induced damage threshold (LIDT) caused by space vacuum (mostly in porous coatings, e.g. deposited by electron beam evaporation technology [5, 6]), laser-induced contamination [5], cryogenic temperature [7, 8];
- Transmission losses caused by contamination build-up or colour centre formation induced by Solar radiation (ultraviolet range) in coatings, low- and high-energy particles (electrons and protons) and gamma radiation in nonlinear crystals [5, 9];
- The erosion of the outer optics of the spacecraft caused by atomic oxygen [5];
- Optics cracking and delamination caused by rapid temperature changes [5];
- Optics displacement or reveal of latent material defects caused by vibrational loads during spacecraft lift off and landing [5, 9].

1.1.2. Mars environment

Pressure on Mars varies from 0,4 to 0,87 kilo pascal (kPa), which is ~0,6% of the atmospheric pressure on the Earth. Laser in MOMA will operate under hermetically sealed protective housing that keeps an atmosphere of synthetic air. This kind of environment is created to reduce the possibility of laser-induced contamination build-up as the composition of the air might have influence on optics contamination [10]. Unfortunately, it is impossible to avoid leakage – air flow from higher pressure environment to the lower one. The mission will be started with 1000 milibar (mBar) pressure in the laser compartment, the predicted pressure in the End of life is 100 mbar. Air composition of Mars: CO_2 – 95,97%; Ar – 1,93%; N_2 – 1,89%; O_2 – 0,146%; CO – 0,0557%. Gravity on Mars is 3,711 meters into squared seconds (m/s^2). Temperature ranges from -133 °C to 27 °C. It is important to take Mars environment into account while deciding design of the MOMA as well as some parameters of LIC measurements [11, 12].

1.2 Laser-induced contamination on spaceborne optics

Taking into account previous experience in space missions and comparing environments of Mars and Earth it is expected to have contamination build-up on optical surfaces of MOMA laser if necessary precautions are not used to prevent it. The presence of contamination in the laser compartment can result in early optical damage under irradiation conditions where it would not normally occur without it. Laser-induced contamination is the formation of deposition layers on optical surfaces due to interaction between intense light radiation, outgassed molecules, especially from organic materials, and optical surface [13, 14]. Schematic drawing of molecular contamination deposition on optics exposed to laser beam in vacuum chamber can be found in Fig. 2. The high-intensity radiation field of the laser tends to attract molecules towards the region of the highest intensity, push and trap them against optical surface and form a deposit.

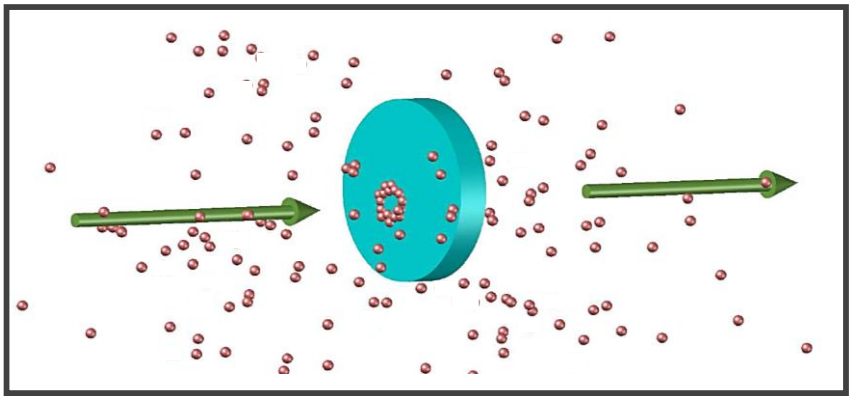

Figure 2. Molecular contamination deposition on optics exposed to laser beam in vacuum chamber.

1.2.1 LIC growth mechanism

Laser radiation interaction with molecules can result in change of the chemical and physical nature of the contaminant [14]. Laser-induced deposit build-up occurs either due to photochemical or photothermal mechanism or both. These mechanisms are triggered by the interaction of outgassing organic constituents with high intensity laser radiation. Photothermal process refers to photoexcitation of material that results in production of heat – thermal energy (e.g. pyrolysis – decomposition of the organic molecules at the elevated temperatures in the absence of an oxidizing environment). Photochemical mechanism could be described as chemical reaction caused by light absorbed by molecules (e.g. polymerization – process during which interacting monomers create polymer chains due to chemical reaction, photolysis - the cleavage of chemical bonds due to sufficient energy of the photon). Under UV exposure contaminants tend to better fixation on the optical surfaces [15, 16] as UV light activates polymerization of the volatile molecules from the outgassing process on the optical surface [17, 18]. As deep UV laser will be used in Mars Organic Molecules Analyser, every precaution must be taken to avoid using materials containing compounds that might cause LIC formation under MOMA laser system working conditions.

1.2.2 The trapping of particles

As it was mentioned before, high intensity radiation field attracts particles towards the region of highest intensity and its pressure forces push and trap them against optical surface. The trapping of particles by the field distribution of a beam could be explained in following manner. For this explanation beam chosen to be Gaussian, refractive index of a particle is greater than its environment, particle is a dielectric sphere [19, 20]. As it is shown in Fig. 3, line marked as B is sphere axis, lines A and C – a pair of beams at equal spacing from B. Beams A and C undergo Fresnel reflection and refraction at the input and output surfaces, as A beam is stronger it determines direction of the dielectric sphere as it is shown in the figure. Radiation pressure forces of the beam A due to reflection at the input and the output surfaces of the dielectric sphere are F_{ri} and F_{ro} respectively, F_{di} and F_{do} are pressure forces due to the refracting beams. The result of these forces of A and C beams makes the sphere to move towards and along the +z axis of the beam [20]. In addition to radiation pressure, if dielectric sphere is placed in an electric field E, it behaves as a dipole. Polarization P of this dipole equals:

$$P = \left[\frac{\left(n_a^2 - n_b^2\right)}{\left(n_a^2 + n_b^2\right)}\right] \times r^3 E = \alpha E \qquad (1)$$

where n_a and n_b are the refractive indices of the sphere and surrounding medium respectively, α is the polarizability of the sphere suspended in the medium, and r is the radius of the dielectric sphere.

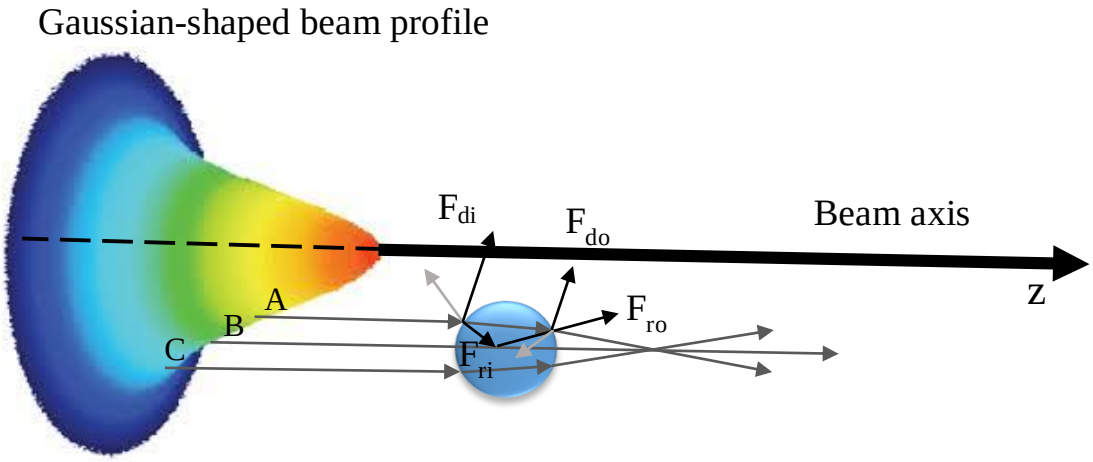

Figure 3. Dielectric sphere driven towards beam axis along +z direction.

In an optical field gradient a force on the sphere, F_{grad}, can be found from equation:

$$F_{grad} = \frac{1}{2}\alpha\nabla(\langle E^2\rangle) \tag{2}$$

where the factor $(\frac{1}{2})$ is a time average over a light oscillation cycle and $\langle E^2\rangle$ is the average of E^2. The force moves the sphere towards the high intensity region if $n_a > n_b$. Furthermore, a force on the particles can be exerted through the squared mean value of electric field $\bar{E}^2$. The electrons or atoms are forced out of the beam field if the frequency of the external field exceeds the frequency of the electron oscillations, the opposite happens at subresonance frequencies. The average force acting on the electrons from the external electric field is:

$$F_{av} = P \cdot \nabla E = (\frac{e^2}{m})\left\{\sum \frac{w_{ok}^2 - w^2}{\left(w_{ok}^2 - w^2\right)^2 + w^2\gamma_k^2}\right\}\nabla\bar{E}^2 \tag{3}$$

where, e and m are electron charge and mass respectively, w_{ok} is the frequency of the resonance, and w is radiation frequency, γ_k is the damping of the k_{th} electron. If radiation frequency is smaller than coupling frequency of the external electrons in the atom $w < w_{ok}$, then the average force will be directed towards the region of high intensity field, consequently particles will move towards the same direction. Furthermore, the electrostrictive pressure induced on electrical non-conducting or dielectric molecules by intense light:

$$p_E = -\rho(\frac{\partial\varepsilon}{\partial\rho})(\frac{E^2}{8\pi}) \tag{4}$$

where, ρ and ε are density of the material and its dielectric constant respectively. The negative sign indicates that the electrostrictive pressure is smaller in regions of high field strength, which means that the molecules will move towards the axis of the beam or the focus [20].

1.2.3 Common contaminants

Generally contaminants fall into two categories: molecular and particulate contaminants. Common particulate contaminants are metallic particles [21]. Interaction with laser radiation might lead to vaporization and plasma formation that results in damage of optical surface. Same effect can be caused by refractory particles such as inorganic oxides and carbon. These contaminants can induce heating centres on optical surface leading to permanent stress fracture or thermal distortion. Due to stronger outgassing rates compared to inorganic materials molecular contamination is mainly caused by organic compounds, e.g. epoxy, adhesives, cable insulating material, multi-layer insulation used for space vehicle thermal control, circuit boards, glue. Examples of molecular contaminants are silicones and aromatic hydrocarbons. Both of these compounds are transparent from the near infrared through the visible wavelength range and yet, silicones and aromatic hydrocarbons are known to induce damage on the optics in 1 μm lasers [20, 21].

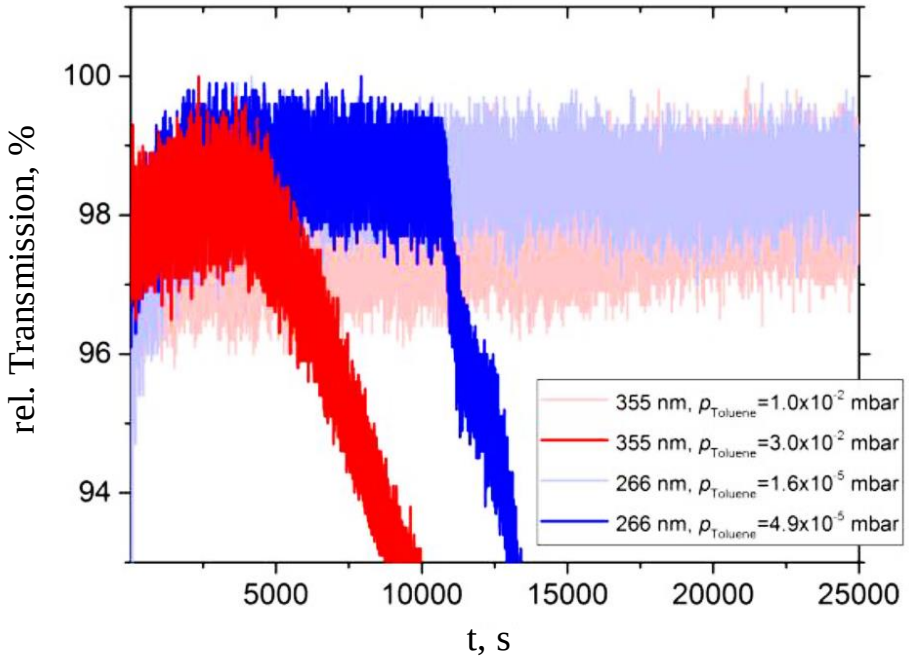

Figure 4. Example of LIC measurement with contaminant – toluene [4]. The transmission gain in the first 2000 – 2500 s is related to the optical surfaces (sample and chamber windows) cleaning.

Another example of molecular contamination is toluene, it has broad absorption band in the range of about 235-270 nm. To estimate toluene's deposition on the optics dependency on wavelength, LIC tests were performed under comparable measurement conditions. Atmosphere in a chamber was created with toluene and nitrogen mixture, and cannot be comparable to natural conditions under which toluene's concentration would be much smaller. As it can be seen in Fig. 4, approximate minimum toluene's concentration at which transmission loss could be detected for 266 nm irradiation is 2-3 orders of magnitude lower than for 355 nm [4]. The results indicate importance of LIC at 266 nm. Compared to the MOMA-laser device, tests were performed under

worst case conditions for LIC growth: extremely high contaminant concentration of toluene, absence of molecular oxygen and high fluence. Further on, choosing materials for MOMA-laser system, compounds containing toluene as molecular contaminant will be avoided in the laser and its components. Depending upon the conditions (wavelength, contamination concentration, oxygen presence, fluence, optical surface, absorption cross section to name a few) contaminants can induce more or less or no harm at all is the laser system. This brings necessity to perform LIC measurements even though only one factor might be different comparing to the similar test.

1.2.4 LIC effect on absorption and laser-induced damage threshold

Laser-induced contamination leads to absorption and reduced laser-induced damage. LIC proved to be particularly critical, if the laser system is operated under low pressure where materials tend to outgas faster [22]. In Fig. 5 example of LIC deposit on the vacuum surface of an optic is shown. During a vacuum test of the Atmospheric Laser Doppler Instrument (ALADIN) laser, the energy dropped by a factor of 2 in 6 hours (h) due to LIC growth on the UV optics [5]. In tests with naphthalene (a partial pressure of 2.4×10^{-4} mbar) at 355 nm it was found that LIDT of AR coated optics is reduced by more than one order of magnitude [23]. Coatings were deposited by Electron Beam Evaporation on fused silica with the top layer of SiO_2.

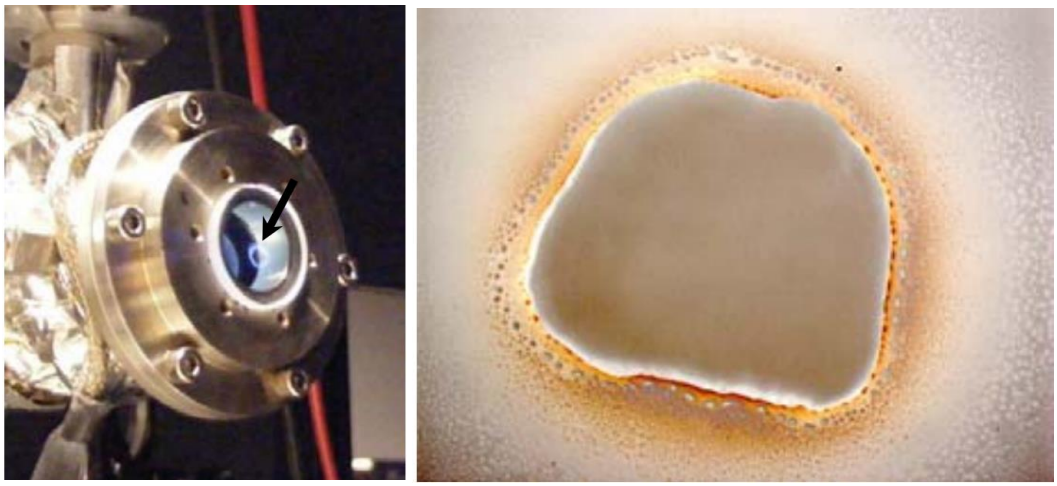

Figure 5. Example of LIC deposit on the vacuum surface of an optic: fluorescence from an LIC deposit on ALADIN optical window at 355 nm (left) and micrograph of an LIC deposit (right) [24].

1.2.5 Gravity effect of LIC

Contamination growth can be induced not only by lower pressure (vacuum) but by weaker gravity field as well [19, 20]. Using simple classical mechanics equations, the Mars gravity effect on LIC can be found:

$$s = vt + \frac{1}{2}at^2 \tag{5}$$

where t – time needed for the object to travel distance (s) at the initial speed (v) with specific acceleration (a). In hypothetical situation in the laser compartment that is on the Earth there is a molecule M_E and there is the same kind laser compartment on the Mars with molecule M_M. Both these molecules are at the same high in the compartment, so they have to travel same distance to settle down on the bottom of laser compartment. Assuming that initial speed is zero (v=0), the eq. 5 can be rewritten:

$$g_M t_M^2 = g_E t_E^2 \quad (6)$$

where $g_{M,E}$ is gravity on Mars and Earth (9,807 m/s^2) respectively and $t_{M,E}$ is the time that molecule takes to settle down. From equation (6) it is seen that molecule settles down on the bottom of laser compartment $\sqrt{\frac{9,807}{3,711}} = 1,63$ times slower (or stays longer in a suspended state) on Mars due to smaller gravity, which means that there is a bigger possibility for molecule to get attracted by the laser beam.

1.2.6 Contamination mitigation

Laser-induced contamination can be critical to the lifetime operation of the laser system situated on board of a spacecraft. The overall long term optical degradation of all laser components eventually will result in irreversible damage of optics and reduced lifetime of the mission. In the ground laser system there is always a possibility to change damaged optical element, there is no such option in space and all possible precautions to avoid laser-induced contamination should be taken. Although LIC is not totally understood, some factors and actions [10, 24, 25, 26] found to be mitigating:

- Selection of suitable materials – screening of harmful materials;
- Preconditioning – vacuum bake-out of materials at temperature higher than the planned operating temperature (although long term outgassing flux will remain);
- Molecular absorbers, cold trappers can be used;
- As molecules tend to condense on the coldest parts of the system it should be ensured that optical components are at higher (or same) temperature than the rest of the system;
- Implementation of a low pressure oxygen environment as it has been shown for 355 nm irradiation oxygen acts as cleaning agent, this cleaning might become even more effective for lower wavelength;
- Heaters could be installed which allow recovery of performance of the optical components via re-evaporation of deposits.
- Laser system should be pressurized and the number of optical surfaces exposed to vacuum minimized.

The precautions taken in MOMA laser system includes careful selection of materials, vacuum bake-out and extended LIC tests prior to flight with all the possible contamination sources. Additionally, laser system is pressurized with synthetic air containing oxygen (O_2), nitrogen (N_2) and helium (He) to 1000 mbar to reduce LIC effect.

1.3 Optics for space applications

The history of spaceborne lasers development is still young and there are a lot of unknown factors regarding the best optical components, procedures, and design for achieving the longest possible lifetime. Behaviour of materials in space environment is not well known till now. Under vacuum or cryogenic temperature conditions, properties of material can change in dramatic rapid ways. Some optical components including coatings and crystalline materials are sensitive to moisture or hydration. Crystalline materials, for example, lithium niobate ($LiNbO_3$) contains interstitial water that evaporates in vacuum. This results in change of $LiNbO_3$ electrical and optical properties which might lead to the system failure. It is clear that this compound cannot be used as non-linear crystal for higher harmonic generation in spacecraft. The removal of the molecular layers from the surface of inorganic solids and metals increases surface energy which leads to changes in the non-linear, linear optical, and dipolar behaviour [9]. To prevent failure of the laser system during space mission it is critical to test the behaviour of the all the parts of the system under space-like environment, even if the manufacturers claim that supplied components are vacuum compatible. In the following sections coatings and bulk materials relevant to MOMA laser system are described in the context of spacecraft environment enhanced issues.

1.3.1 Coatings

For past few decades coated surfaces have played an important role in laser technology. Coatings allow to manipulate laser beam in different manner: splits the beam in certain proportions, filters unwanted wavelength range or specific wavelength, increases reflectivity or transmissivity to almost 100 %, polarizes light to name a few.

1.3.1.1 Effect of deposition techniques

Porous coatings such as evaporatively deposited coatings or sol-gel coatings are more likely to change when situated in vacuum. Water evaporation in these coatings under vacuum induces changes in the composition of the surface resulting in surface stress change from compressive to tensile, spectral shift to lower wavelengths and reduction of LIDT [5, 6, 27]. Vacuum effect on laser-induced damage threshold in porous and dense coatings can be seen in Fig. 6. LIDT of dense

coatings (deposited by: Ion Assisted Deposition (IAD), Ion Beam Sputtering (IBS)) in ambient and vacuum conditions varies just by few percent, LIDT of coating deposited by Electron Beam Evaporation (e-Beam) for 1 pulse decreases by around 25% and for 1000 pulses – more than 60%.

Another space-like environment effect dependent on the coating deposition technique is laser-induced contamination [23]. In Fig. 7. It can be seen that during LIC measurements fluorescence signal is much higher for E-beam sample. This means that deposit on this sample is bigger in volume than on sample coated by Magnetron Sputtering (MS) deposition or uncoated fused silica. Similar measurements were performed with IBS coatings which showed much worse contamination than MS deposited coatings [28]. Clearly formation of depositions depends on the surface design of the optical samples as well as on its chemical composition: magnesium fluoride (MgF_2) coated optics the deposition growth rate was 2 – 3 times larger than on silicon dioxide (SiO_2) coated ones [17].

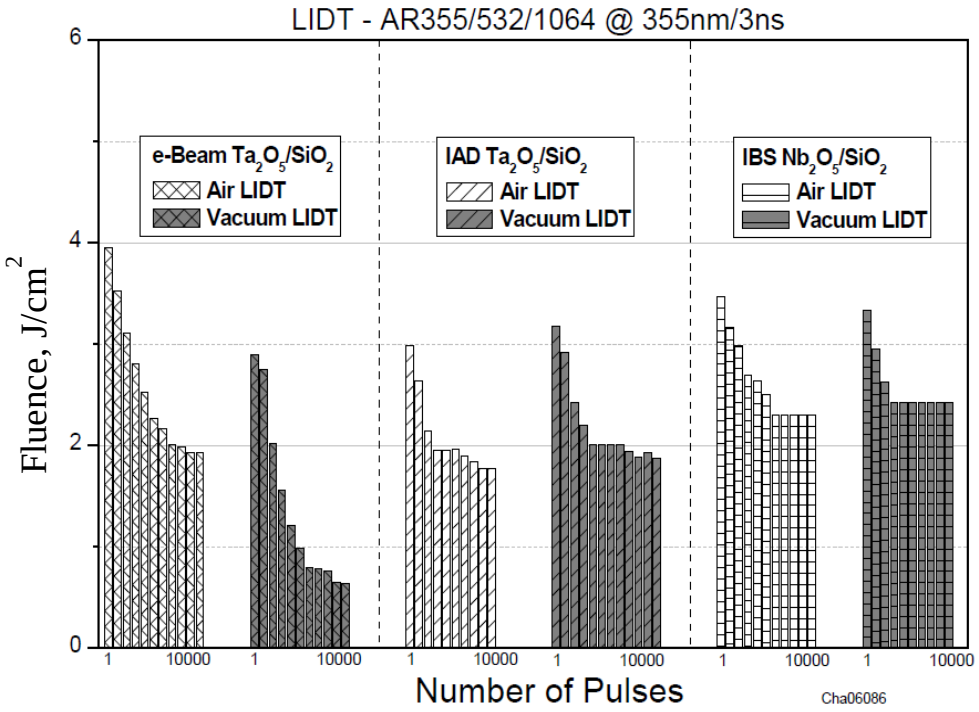

Figure 6. AR coating results for air and vacuum tests of the LIDT at 355 nm wavelength and 3 ns pulse width [6]. Materials used for e-Beam and IAD coatings: Tantalum pentoxide (Ta_2O_5) and silicon dioxide (SiO_2), for IBS coating: niobium pentoxide (Nb_2O_5) and SiO_2.

MS deposition technique was chosen to produce AR coatings for MOMA laser as it has good performance in vacuum: constant LIDT and smallest contamination. Magnetron sputtering deposition technique is described in detail in the following section.

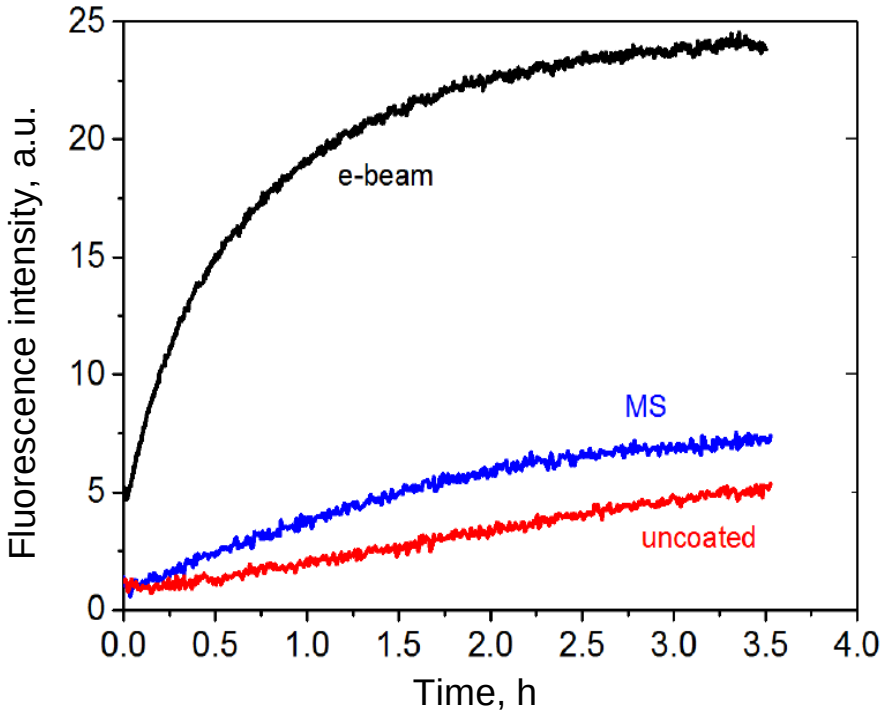

Figure 7. In-situ monitored fluorescence signal intensity dependency on exposure time for AR coated samples and uncoated fused silica. Peak fluence: 7 mJ/cm². Repetition rate: 1000 Hz. Test wavelength: 355 nm. Contaminant – naphthalene, its pressure – 3.5×10^{-4} mbar [23].

Magnetron sputtering deposition

In terms of quality, performance, and cost magnetron sputtering stands in between evaporative and IBS techniques. The advantages of Magnetron Sputtering includes: excellent layer uniformity, smooth and dense coatings, higher deposition rates than IBS, non-conductive materials are sputtered by using radio frequency or medium frequency power, almost all metallic target materials can be sputtered without decomposition, high flexibility of sputtering equipment design. The equipment design and deposition procedure depends on the desired target materials and coating parameters. One of the main disadvantages is that the target source is much closer to the substrates than in other processes and in some cases, for example for components with a steep radius of curvature, it leads to worse surface quality and uniformity comparing to IBS deposition technique. Another disadvantage comparing to IBS is the difficulty to control deposition parameters [29].

Sputtering in general is a physical vapour deposition (PVD) process that is used for materials deposition onto a substrate. Atoms are ejected from target materials and condensed onto a substrate. The principle of Magnetron Sputtering using metal as a target material is shown in Fig. 8. The target material is connected to negative electrode and immersed in a magnetic field. Plasma, typically consisting of inert gas ions such as Argon (Ar^+), is created above the negatively charged target. Positively charged ions are accelerated towards cathode due to its negative potential. The impact of these ions with the target cause atoms to be ejected – sputtered off. The energy of ions is

sufficient to release electrons, which are trapped by the magnetic field. Electrons are accelerated towards anode and colliding with neutral gas atoms ionizes them and maintains the plasma above the target. The ejected atoms from the source material are neutral and travel towards substrate unaffected by magnetic field. Atoms condense on the substrate and bind to each other at the molecular level, forming a dense atomic layer. One or more atomic layers can be deposited depending on sputtering time. It allows the precise production of the thin films. Densely packed atomic layers result in little or no spectral shift that is common in porous coatings due to absorption of atmospheric moisture. To avoid contamination during deposition process sputtering takes place in the vacuum environment, only inert gas for plasma creation is introduced into a vacuum chamber at a pressure of 1 – 10 mbar [30, 31, 32].

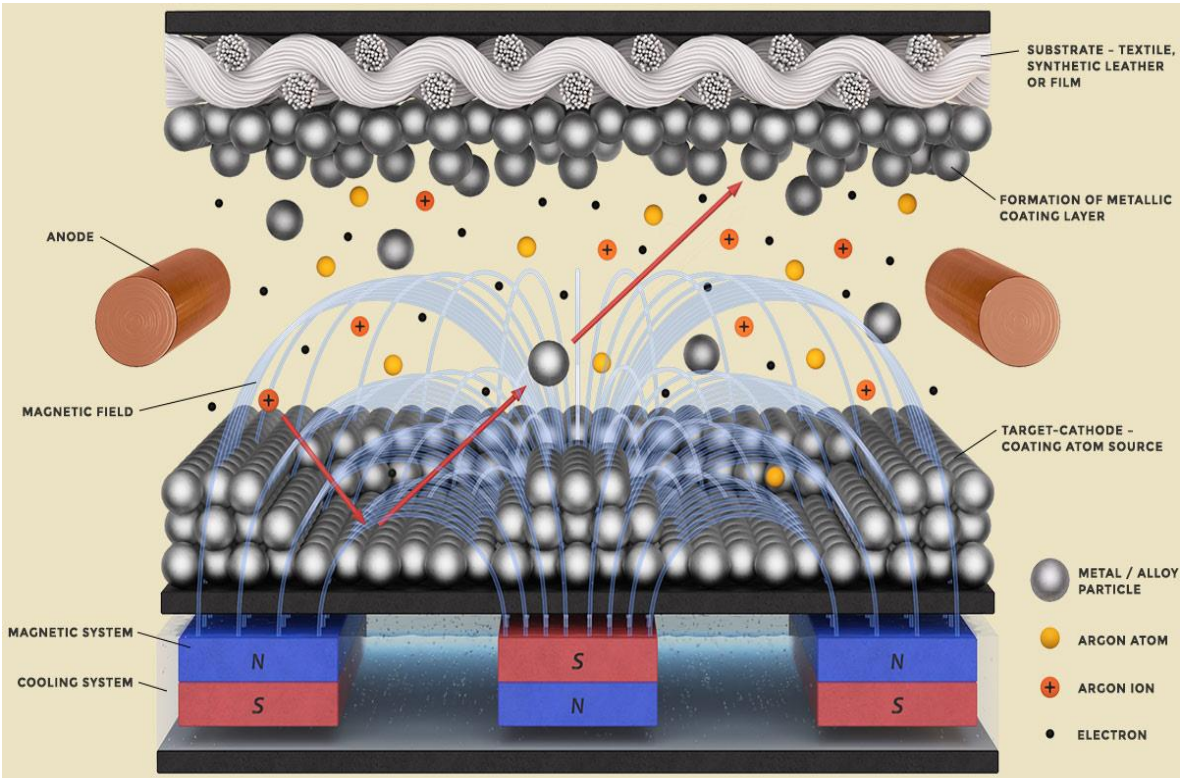

Figure 8. Principle of Magnetron Sputtering [33].

1.3.1.2 Coating designs

Many different coating designs are known: antireflective (AR), high-reflective (HR) coatings, partial reflectors, non-polarizing or polarizing beam splitters, filters for monochromatic, dichroic, and broadband applications and so on. In the context of LIC or, to be more precise, contamination induced damage, two coating designs were compared: AR and HR. As it can be seen in Fig. 9 the transmission of AR coated sample got reduced from the beginning of the measurement, while there is just slight reduction in HR coated sample reflectance under the same condition. Ex-situ inspection confirmed that transmission reduction of HR coated sample is due to LIC build-up and AR coated sample got

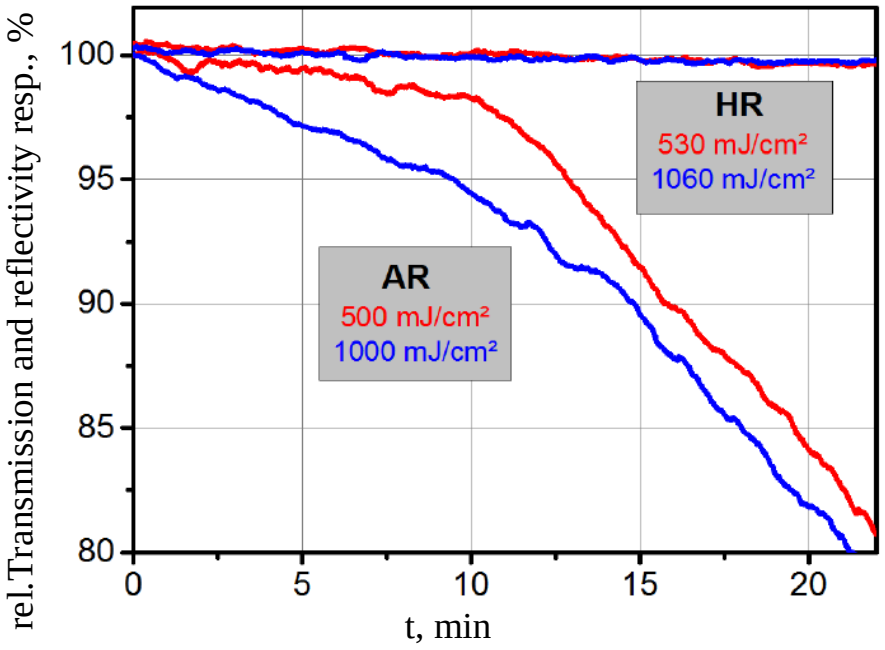

Figure 9. Transmission and reflectivity as a function of irradiation time for AR and HR coatings respectively (e-beam deposition). Contaminant (naphthalene) pressure: 10^{-4} mbar, test wavelength: 355 nm [23].

damaged even though the LIDT in vacuum for this coating is 7,5 J/cm^2. Additional in-situ technique – laser-induced fluorescence monitoring allows to confirm that there was laser induced contamination build-up before sample got damaged [23]. This shows that contamination growth is more severe for AR coated samples.

Principle of anti-reflective coating

The principle of AR coating operation is described in detail below as this coating design is of interest to this research. The light wave reflected from two interfaces interfere either constructively or destructively depending on mutual phase difference between both reflected waves. In Fig. 10. operation of multilayer dielectric coating is shown.

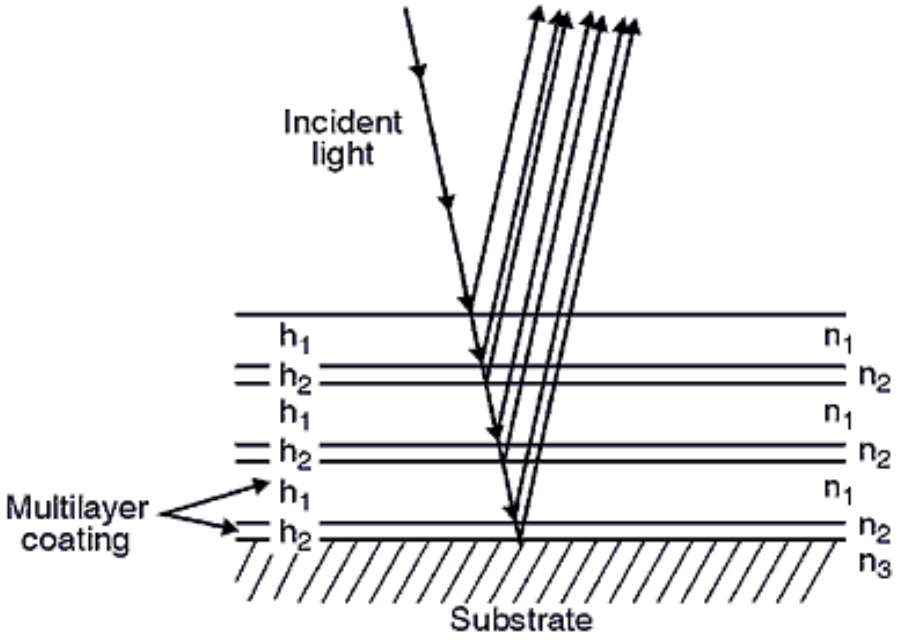

Figure 10. Operation of a multilayer anti-reflective dielectric coating [34]. $n_2 > n_1$

Coating consists of alternating layers of thickness h_1 and h_2 with indexes of refraction n_1 and n_2, optical thickness (the product of the refraction index and thickness of the layer) of each layer equals to quarter of the wavelength ($\frac{\lambda_o}{4}$). In this case reflected light interfere destructively. Two wave reflected from first two interfaces (air-first layer and first-second layers interfaces) already has a phase shift of π as both are reflected from more dense layer. The optical path difference for the light incident perpendicularly to the surface for the case shown in the drawing:

$$2n_1h_1 = \frac{\lambda_0}{2} \tag{7}$$

Light reflected from the second interface gains phase shift of π while propagating in the first layer of the coating, so the phase difference between two interfering waves is π as well, so these waves interfere destructively. The general equation for destructive interference:

$$2nh\cos\theta = (m+1)\frac{\lambda_0}{2}\ ,\ \ m = 0, 1, 2, 3\ldots \tag{8}$$

where, θ is the angle of incidence of light. For the same design to work as a high reflective coating layer of thickness h_2 and refractive index n_2 should be added on the top.

1.3.2 Substrate

There is no specific data on substrate degradation, nor on what kind of substrates have better performance in space environment. Although it has been noticed that high energy radiation, e.g. UV, can induce colour centre formation in the optics [5]. During measurements on the ground with wavelength of 266 nm optical components made out of UV grade fused silica showed degradation. As degradation of the optics have huge impact on sensitivity of performed tests relevant fused silica properties are described in the next section.

1.3.2.1 Fused silica degradation at 266 nm

Fused silica or fused quartz consists of silica in amorphous form. The high-purity fused silica is comprised of perfect $Si(O_{1/2})_4$ tetrahedrons joined at the corners with Si-O-Si and dihedral angles, as it is shown in Fig. 11. a). In amorphous fused silica closed rings with varying numbers of members are formed out of three and more tetrahedrons [35, 36].

It is hard to produce perfectly transparent fused silica for deep UV applications especially where high fluence is used. Comparing three kinds of UV grade fused silica it was found that when exposed to 266 nm radiation it exhibits different levels of degradation, for example E' centre creation [37, 38]. Besides creation of new defects fused silica exhibits many other point defects, its absorption bands are shown in Fig. 12. Defects responsible for 266 nm radiation absorption are Non-Bridging Oxygen Hole Centres (NBOHC) and Oxygen Deficient Centres (ODC). NBOHC has broad emission band with canter at around 650 nm (red fluorescence), while

ODC – 420 nm (blue fluorescence). Intrinsic point defects that absorb at 266 nm and induced defects by 266 nm laser radiation in fused silica are shown in Fig. 11.b).

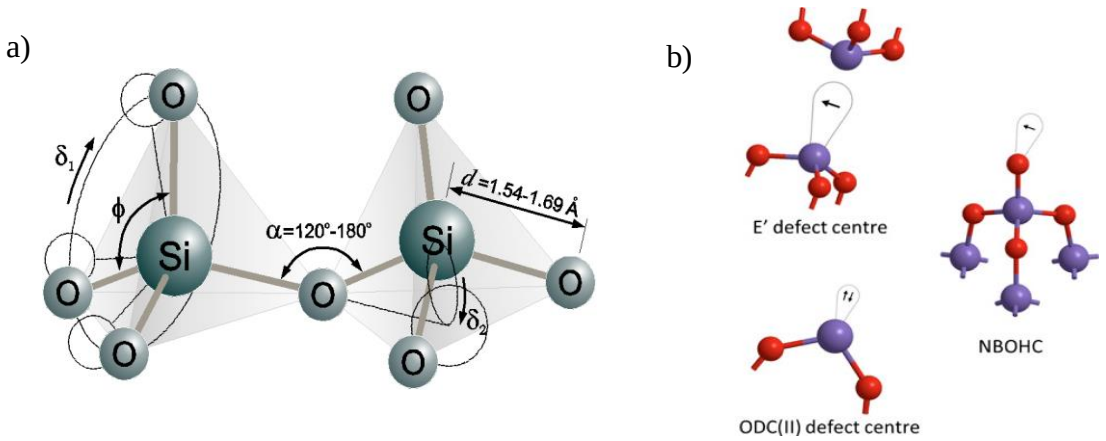

Figure 11. Three-dimensional schematic of a) pure fused silica [36], b) point defect (E' centre) induced by and intrinsic defects that absorb at 266 nm in fused silica [39].

Additionally, bulk scattering losses and proportional to $\frac{1}{\lambda^4}$ and are much bigger comparing to losses in the visible or infrared range [35]. Recording transmission spectra of fused silica component, fluence might be too low or interaction time of laser radiation with matter too short to induce colour centres or the absorption of intrinsic defects might be misinterpreted with scattering losses or Fresnel reflection. This leads to conclusion that before using UV grade fused silica it has to be tested in the working conditions.

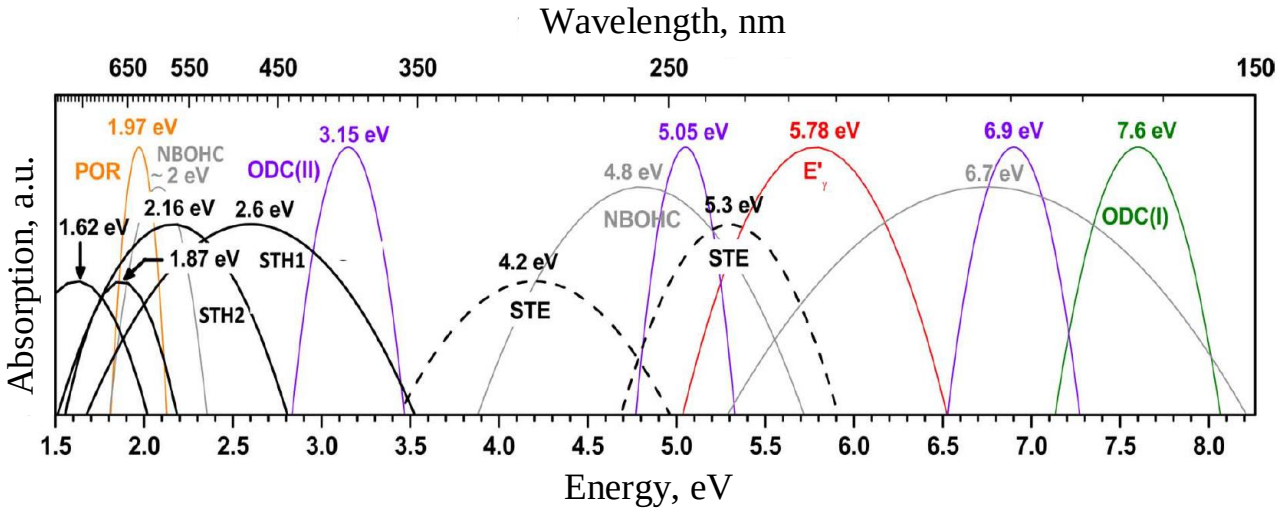

Figure 12. Absorption bands associated with different Silicon-related point defect structures. POR – Peroxy Radicals, STH – Self-Trapped Holes, STE – Self-Trapped Excitons [40].

2. Experimental procedure

2.1 Preparation of optical samples

For laser-induced contamination measurements AR-coated UV grade fused silica with protective-top-layer is used. Optic is designed for wavelength of 266 nm and fabricated by Magnetron Sputtering technique. The design and materials of the optics are classified. The specimen's coating resembles AR coating used in real MOMA laser system. Transmission spectra of the optical sample is plotted in Figure 13. Transmission at the wavelength of 266 nm is 99,62%.

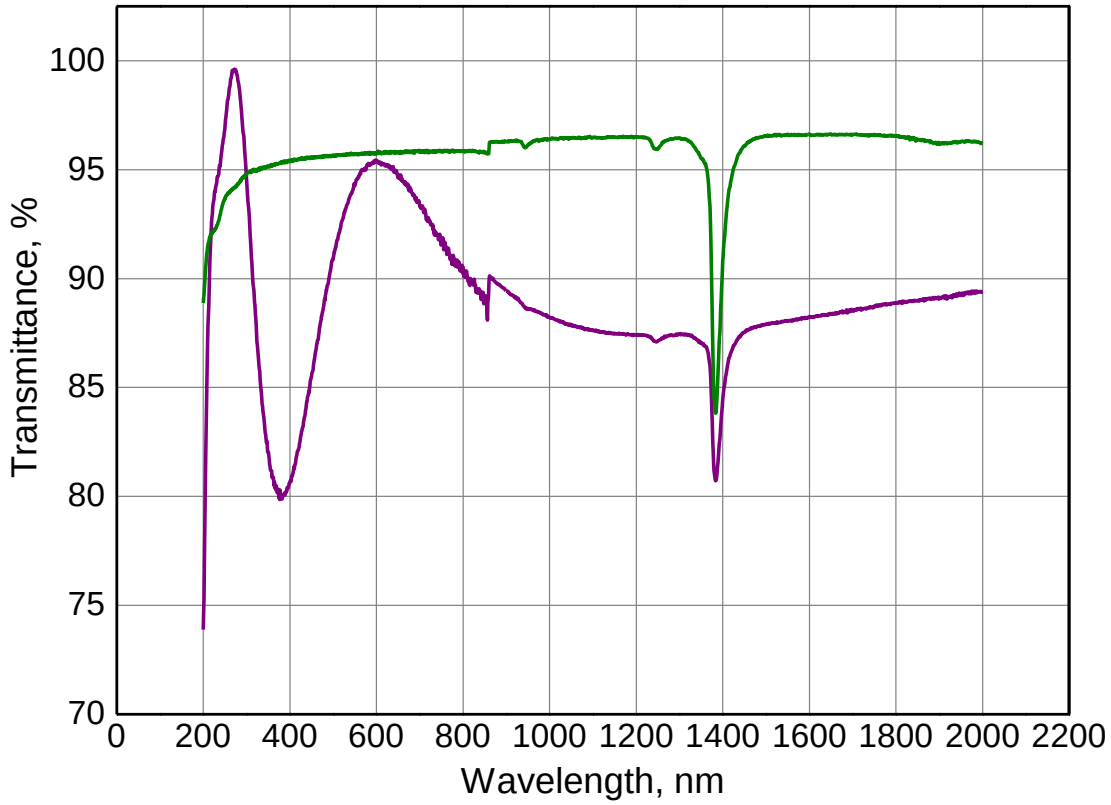

Figure 13. Transmission spectra of specimen (purple line) and standard UV graded uncoated substrate [41] (green).

Prior to the measurements the specimen needs to be cleaned. For dust and particle removal the optical sample is placed under stream of dry pressurized nitrogen. Then the sample is cleaned by drop and drag method using extra pure acetone. To be sure that the specimen is clean it should be inspected by Differential Interference Contrast (DIC) microscopy. If needed, the cleaning procedure can be repeated few more times.

2.2 LIC test bench

2.2.1 Optical setup

In order to perform LIC tests for spaceborne optics a test bench has been assembled. Principal optical setup is shown in Fig. 14 and three-dimensional test bench in Fig. 16.

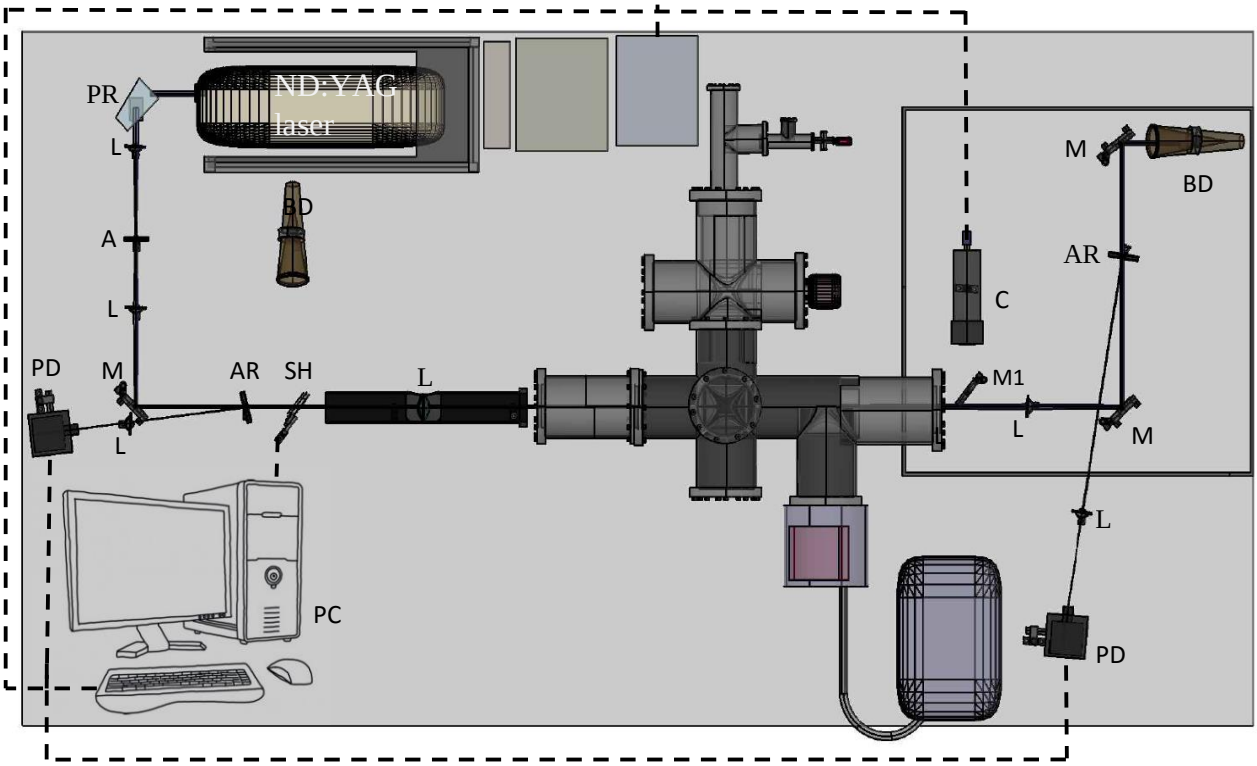

Figure 14. Laser-induced contamination optical test bench.

Optical test bench components: PR – Pellin Broca prism, L – lenses, A – aperture, M – high reflective mirrors for 266nm wavelength, PD – integrating spheres, AR – substrate coated with anti-reflective coating, BD – beam dump, M1 – mirror, C – camera, PC - computer.

Laser source used for the measurements is Q-switched neodymium-doped yttrium aluminum garnet (Nd:YAG) laser produced by Continuum (Minilite II). It produces wavelength of 266 nm by increasing its fundamental frequency fourfold using two nonlinear crystals. It has repetition rate of 10 Hz and pulse width of 5,3 nanoseconds (ns). For controlling laser output power optical attenuator, consisting of half-wave (λ/2) plate and polarizer, is placed in the laser compartment. The power can be changed without or with small effect on beam profile. Pellin Broca prism in front of the laser is being used for second and fourth harmonics separation and laser beam deviation (only one wavelength – 266 nm) by 90 °C, schematic drawing of laser beams with the wavelengths of 266 and 532 nm propagation through prism is shown in Fig. 15.

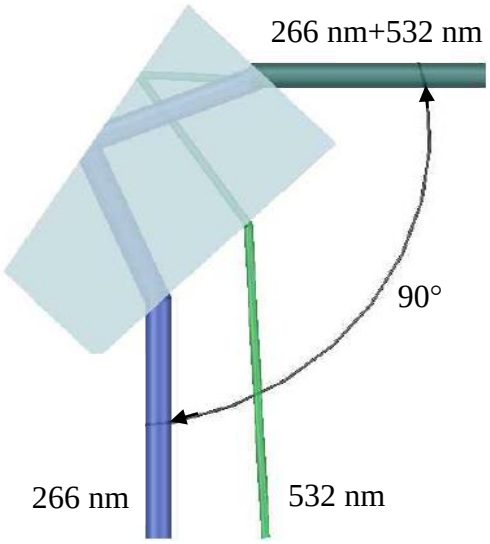

Figure 15. Schematic drawing of Nd:YAG laser's second and fourth harmonics propagation through Pellin Broca prism.

For the pulse energy measurements a part of the beam is coupled out by AR coated substrate. This part of the beam is detected by integrating sphere, which spatially integrates incident radiant flux. To insure high fluence on the sample, lens in front of the chamber is used. For transmission signal detection same kind of optics and detectors are used as for reference signal. Camera after the vacuum chamber is used for laser-induced fluorescence of the contaminant on the sample imaging.

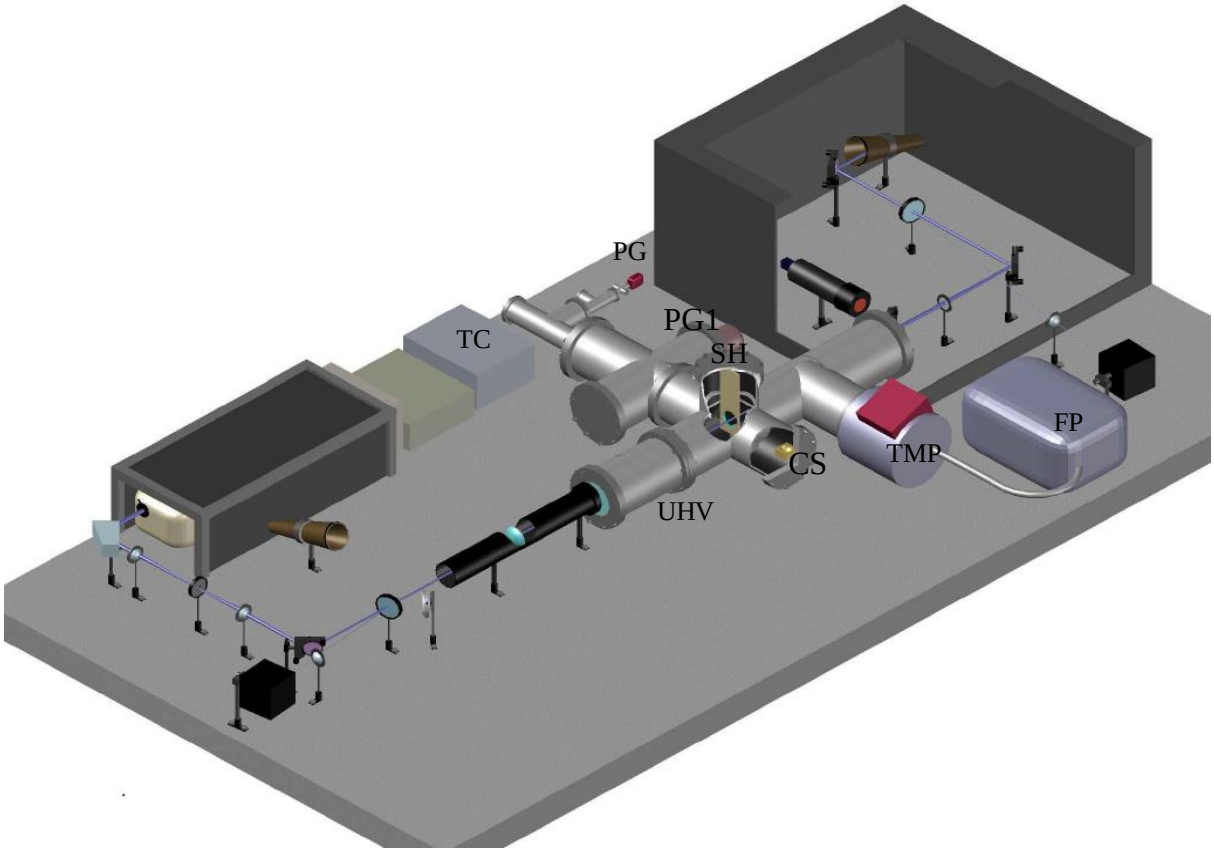

Figure 16. Principal LIC test bench for space born AR coatings (3D view).

LIC test bench contains: UHV – ultra-high vacuum chamber, CS – contamination source, SH – sample holder, PG and PG1 – pressure gauges, TC – temperature controller, FP – forepump, TMP – turbo molecular pump.

Spaceborne laser environment is simulated in ultra-high vacuum chamber (UHV). Ultra-high vacuum is created by using oil-free forepump (Pfeiffer MVP 040-2) and turbo molecular pump (Pfeiffer HiPace 80). Pressure up to 10^{-8} mBar can be reached. For pressure sensing in the vacuum chamber two pressure gauges manufactured by Pfeiffer Vacuum are used: Pirani gauge for pressures in range of $5*10^{-2}$ – 1500 mbar and Pirani combined with cold cathode gauge for sensing $6{,}6*10^{-9}$ – 100 mBar. As it mentioned before, in the beginning of the mission the laser is pressurised to 1000 mBar atmosphere with synthetic air to mitigate contamination growth on optics that is exposed to laser radiation, but due to the leakage in the End of life of the mission pressure in the laser compartment is expected to drop tenfold. As the outgassing rates of materials are bigger at lower pressures it was decided to test the worst case scenario. Simulated environment in UHV chamber includes pressure of 100 mBar of pure air, known as synthetic air as well. The air mixture used in this experiment consists of 79% of N_2, 20% of O_2 and 1% of He. As molecules tend to concentrate on colder parts of the system, sample holder is held at 0 °C temperature with the help of Peltier element. Contamination source during the measurements is placed in the oven, which is heated up to 60 °C (or higher in some cases), to speed up outgassing of the contaminants. Temperature controller TC200 (Thorlabs) is used for stabilizing temperature of laser. Main test parameters for LIC measurements are included in the Table 1.

Table 1. Test parameters for LIC measurements

Laser wavelength	λ = 266 nm
Pulse duration	τ = 5,3 ns
Pulse repetition rate	f_p=10 Hz
Beam diameter in the target plane	D_{eff} = 230 μm
Pulse energy	E_p = 2,5 mW
Angle of incidence	$\theta = 0^\circ$
Temperature of contaminant	T = 60 °C
Coating of optical sample	AR
Fluence	0,6 J/cm^2
Pressure in the chamber	100 mBar
Temperature of sample holder	T = 0 °C
Temperature of the oven	T = 60 °C
Dimensions of cylinder shaped optical sample	H = 6,35 mm, D = 25,4 mm

2.2.2 Contamination monitoring units

2.2.2.1 In-situ

In the following section instruments that are used during LIC test for online data monitoring are described. These include: in-situ transmission measurements and laser-induced fluorescence (LIF) monitoring.

Transmittance

In-situ transmission signal measurements are of big importance for detecting contamination deposition on the sample. Contamination build-up might change optical features of the sample quite drastically as it increases scattering and/or absorption of the laser signal by the sample. If contaminants absorb in the range of the laser wavelength, it causes big transmission signal losses and it is good indication of contamination build-up, and in some cases its dynamics. In previous measurements using 355 nm laser radiation it was found that just few nanometer thick contamination build-up causes significant transmission losses in the UV range [10, 42].

As can be seen in Fig. 14 the forth harmonic of Nd:YAG laser beam is entering the chamber as well as the sample plane and exit window at 0° angle of incidence. The same laser beam that induces contamination build-up on sample surface has a role of probe beam as well. The moment contaminants start to form a deposit on the sample, energy of the laser beam behind the chamber starts to drop (if contaminants have absorption band in the range of the laser wavelength). To see if there is a drop in the signal due to new absorption and scattering centres, the ratio of the laser beam energy before and after the chamber is monitored. The optical set-up is divided in to two parts: reference arm (all the optics till the shutter) and transmission arm (the rest of optical components). For energy monitoring in both arms a small portion of the beam is coupled out by the AR coated fused silica substrate which is proportional to the laser beam energy. Reference signal not only allows to detect laser beam energy drop through the time due to contamination build-up, but compensates changes in the laser output power that is described more in detail in the following sections. The most informative plot in the LIC measurements is (normalized) power ratio of reference and transmission signals:

$$t = \frac{a * U_1 + b}{c * U_2 + d}; \tag{9}$$

where a, b, c and d are coefficients found from calibration curve (average power as a function of voltage), U_1 and U_2 are transmission and reference signals (Volts) respectively. To normalize the power ratio all of t values are divided by its maximum value. From normalized ratio plot one can

easily see transmission signal drop in percentage. Even though in LIC measurements only the change in power ratio has meaning, transmission losses due to Fresnel reflection, scattering and absorption by optics needs to be taken into account while calculating fluence on the sample plane.

Laser-induced fluorescence

The measurements are performed with deep UV laser that not only induces contamination build-up on optical surface but serves as excitation source for fluorescence of the deposit as well. At this wavelength range the cross section of excitation of many organic molecules is large and fluorescence signal of the deposits on the optical surfaces is a good indicator for LIC tests [43]. Laser-induced fluorescence can be described as light emission from molecules excited to singlet states by absorption of laser electromagnetic radiation. Laser-induced fluorescence is very sensitive method for contamination build-up detection. In some cases (for 355 nm radiation), deposit layers with a thickness of few tens of nm can be detected [10, 17].

LIF monitoring enables 2D imaging, additionally, as fluorescence signal is proportional to deposit thickness [43] it would be possible to find approximate build-up rate for a specific spot of the deposit. Fluorescence pictures are recorded in time intervals Δt = 1 min. To avoid fluorescence from fused silica substrate and interference from scattered light corresponding filter should be mounted in front of the camera's focusing optics. Images are taken with the "Basler acA2000-340kc Camera link" camera with the CMV2000 complementary metal oxide silicon (CMOS) sensor that delivers 340 frames per second at 2MP resolution.

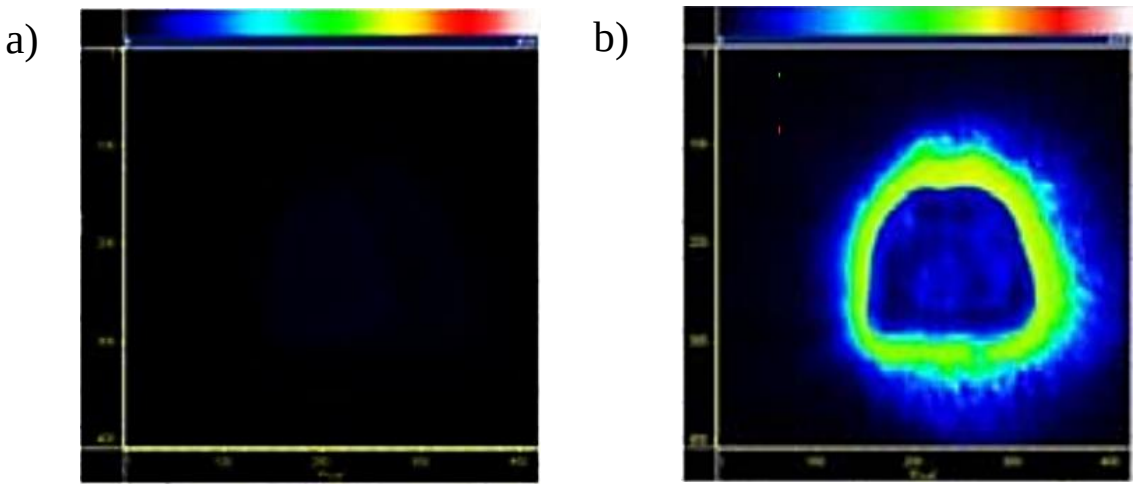

Figure 17. Example images of laser-induced fluorescence recorded during LIC test (λ = 355 nm), picture taken in a) the beggining of measurement, b) after 65 hours (so called doughnut-shaped deposit) [24].

As it is seen in previous LIC tests the shape of deposits highly depends on laser beam profile and fluence. In the beginning of contamination build-up deposit looks like pancake and later it starts to resemble doughnut as cleaning takes place at the region of highest fluence that exceeds the

threshold value (pulsed 355 nm laser), or continues grow in a pancake shape (for continuous wave 375 nm laser diode) [25]. In Fig. 17, example images of laser-induced fluorescence recorded during LIC test are shown. If fluorescence signal is directly proportional to the thickness of the deposit, than summed fluorescence signal should go down a bit when the cleaning process starts and then go up as the outer part of the deposit keeps growing.

2.2.2.2. Ex-situ

Differential Interference Contrast Microscopy

When LIC measurements are over, specimen is examined with Differential Interference Contrast microscopy also known as Nomarski microscopy. Nomarski made DIC possible by modifying the Wollaston prism that is used for detecting optical gradients in samples and converting them into intensity differences. Contamination build-up can be seen only in two dimensions: only shape and size of deposit can be approximately determined, but not the depth. Nomarski microscopy is a method to visualize differences in optical path lengths which allows the investigation of transparent samples. The peaks and troughs seen in the image are the product of the optical gradient through the deposition on optical sample and the wavefront path distance.

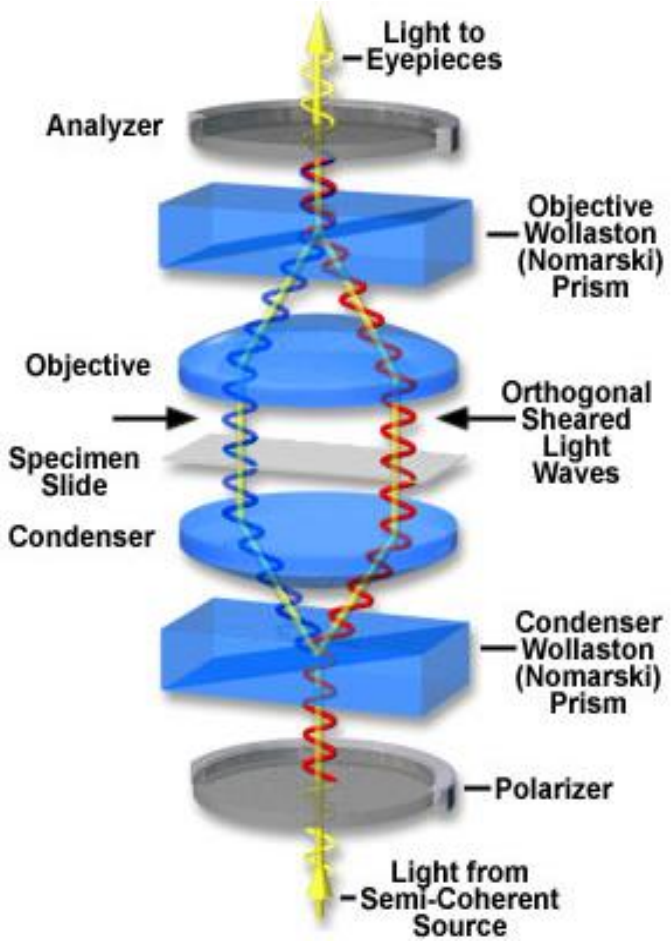

Figure 18. Schematic drawing of light propagating through DIC microscope [44].

The basic principle of Differential interference contrast microscopy (Fig. 18): the light from the lamp (unpolarised light source) propagates through a standard polarizer, producing plane-polarized light. Polarized light is split into two beams (ordinary (o) and extraordinary (E) rays) traveling in slightly different directions by modified Wollaston prism (different Wollaston prisms are used for objectives of different magnification). The two wavefronts pass through the sample where

each component undergoes shift in its phase depending on the thickness and refractive index (n_e differs from n_o) of the specimen for each component. Light beams are focused into second modified Wollaston prism where both components recombine and interfere with each other. Finally the analyser blocks directly transmitted light and the rest of the light is imaged onto the camera. Phase shifts of the e- and o- rays become visible by the variations of colour or intensity [45].

2.2.3 Vacuum system

Vacuum chamber is one of the most important elements in LIC test bench. It has volume of 5,3 l. UHV chamber is made out of stainless steel and consists of 11 CF flanges which allow mounting of a sample holder and oven for contamination source (Fig. 19) as well as monitoring and controlling its temperature, connecting turbo molecular pump and pressure gauges, two flanges parallel to each other contain laser beam entrance and exit windows that are AR coated for a wavelength at 266 nm. One of the UHV chamber flanges is connected to a gas bottle of pure air, chamber can be purged and tests can be performed under different pressures. The turbo molecular pump can evacuate the chamber down to 10^{-8} mBar within 16 hours. Additionally, a mass spectrometer can be integrated for determination of the composition of contaminating material. Most of the flanges are sealed using copper gaskets to minimize possible chamber contamination by introduction of organic materials to the system. Only laser beam entrance and exit windows are sealed using thoroughly cleaned and baked-out Viton®-seals (O-rings). Installed gate valve separates vacuum pumps and the rest of the chamber as some of the possible contaminants are floating back from the barrels after pumps are turned off. Additionally, metal sealed fine control valve in used for air inlet.

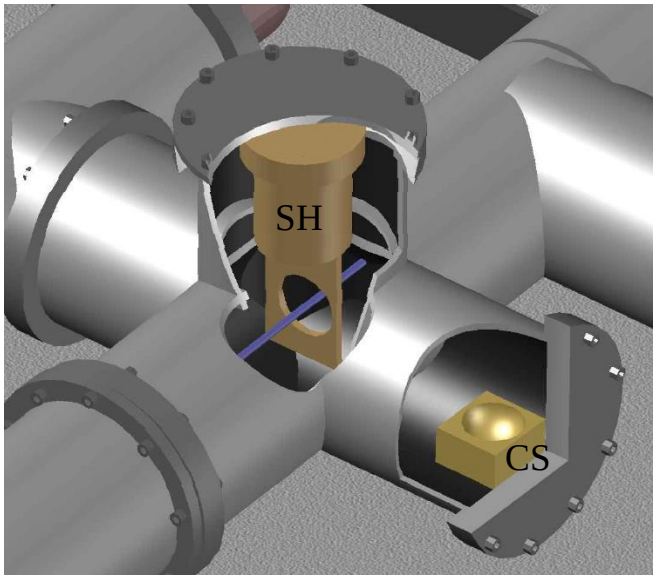

Figure 19. Schematic drawing of mounted sample holder (SH) and oven for contamination source (SC) in the vacuum chamber.

2.2.4 Contamination sources

Contamination sources are mounted on the oven that is situated in the vacuum chamber. Contaminants were supplied by Laser Development Department of LZH responsible for MOMA laser design and its construction. Some parts of the MOMA laser needs to be tested whether it contaminates the optics or not. As it was mentioned before contamination build-up might shorten the life time of

the mission very drastically, it brings the necessity to choose materials and the way it is prepared very carefully.

First contamination source – epoxy “Loctite Ablestik 2151” known as “TRA-BOND 2151“. On one hand, most of the epoxies are known to outgas under the vacuum conditions, on the other hand, the outgassing can be reduced by proper bake-out. “Loctite Ablestik 2151” is a thixotropic, two-part adhesive that develops strong bonds at room temperature. Preparation of the sample was made the same way as it would be prepared for using in MOMA laser: first resin and hardener were mixed and cured for 24 hours at room temperature and then it was baked-out at elevated temperature for another 24 hours to slow down outgassing rate. “Loctite Ablestik 2151” passes NASA outgassing standards where the outgassing behaviour of materials is characterized by the parameters CVCM (collected volatile condensable material), TML (total mass loss) and WVR (water vapour regained). The values of these parameters for some of the materials can be found in NASA „Outgassing Data for Selecting Spacecraft Materials“ [46].

Table 2. Properties of epoxy “Loctite Ablestik 2151”

Property	Typical Value
Mass of contamination source	2,5 g
TML	0,55%,
CVCM	0,03%
WVR	0,22%.
Thermal conductivity	0.95 W/M °K
Coefficient of Thermal Expansion	26 ppm/ºC
Mix ratio (resin/Hardener)	100/9.5
Reactive solids contents	100%
Operating Temperature	-70 to 115 °C
Glass Transition Temperature	60 °C

Second contamination source – electrical plugs (3 units) that might be used in MOMA laser in case plugs that do not contain any outgassing materials do not work (it might not survive the mechanical demands or the pins within the plugs loosen up during vibration test). These alternative components contain low-outgassing epoxy material. All the properties that listed for first contamination source are classified. Before LIC tests, plugs were baked-out at elevated temperature for 24 hours to slow down outgassing rate.

2.3 Measurement plan

2.3.1 System preparation

2.3.1.1 Beam profile characterization

Beam profile on the sample surface was measured by a charge-coupled device (CCD) camera fitting a density profile on the spatial profile. Software from "Spiricon" is used to fit the waist to $1/e^2$ intensity of the beam. To prevent saturation of sensors, corresponding filters are used in front of the CCD camera. The beam profile is taken placing mirror in front of the UHV chamber and CCD camera at the distance equal to the distance between mirror and sample. The measured beam profile at the sample plane is shown in Fig. 20. The beam profile is more elliptical than Gaussian beam shape. For LIC test effective beam diameter is calculated using equation:

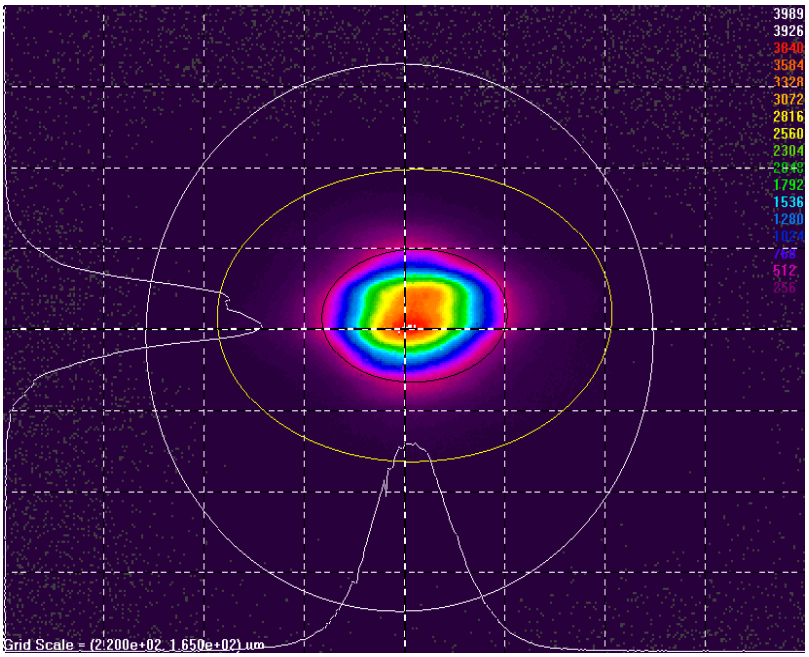

Figure 20. Beam profile at sample plane.

$$D_{\text{eff}} = \sqrt{(a * b)} \tag{10}$$

where a, b – diameters on major and minor axes respectively. Effective beam diameter D_{eff} = 230 micrometers (μm).

2.3.1.2 Estimation of peak fluence

During the measurements the ratio of the fluence on the chamber windows and sample plane is kept in the range of about 1:1000 to avoid contamination growth on the windows. For laser-induced contamination measurements fluence H chosen to be the same as in the MOMA laser system and it is equal to 0,6 J/cm^2.

Laser fluence can be defined as energy delivered per unit area:

$$H = \frac{E}{A_{\text{eff}}} = \frac{4 * E}{\pi D_{\text{eff}}^2}; \tag{11}$$

where E – pulse energy, A_{eff} – effective surface area. Pulse energy can be calculated from average power P_{av}:

$$E = \frac{P_{\text{av}}}{f_{\text{p}}}; \tag{12}$$

where f_{p} – pulse repetition rate.

2.3.1.3 Vacuum system preparation

Before every measurements vacuum chamber needs to be cleaned thoroughly, it minimizes the risk of cross contamination by contaminant from previous tests. The most efficient way is to bake-out the vacuum chamber by heating it up from outside while pumping outgassing products out. By applying heat on the chamber walls rate of outgassing is being accelerated and it results in faster cleaning of the chamber. Electrical heating bands are used as a heat source – the camber is wrapped with it to ensure homogenous temperature profile. It is advisable to heat out the chamber for 24 hours or more. Beam entrance and exit windows has to be cleaned the same way as specimen. O-rings should be changed or properly cleaned and baked-out after every positive LIC measurement as from previous works it has been noticed that contaminants can collect behind it. Viton®-seals needs to be baked-out in the oven prior to its installation. After bake-out the pressure in the chamber should be lower than 10^{-8} mbar and blank test (zero measurement) should be performed thereafter to ensure that there is no contaminants left in the vacuum chamber. Before performing measurements vacuum chamber is being purged and evacuated at least three times. For purging as well as for creating desired atmosphere for test pure air, is used.

2.3.2 LIC investigation process

As optical setup is sensitive to temperature change and some of the optical components degrade exposed to 266 nm radiation, LIC test bench characteristics were highly considered creating laser-induced contamination measurement procedure. LIC measurements are done in following order:

1) As it takes around 5 hours for laser signal to get stabile, it should be turned on in the morning as well as laser heater has to be enabled (33 °C). As LIF signal rises with increasing temperature of camera (the temperature has large influence on the sensitivity of the chip), measurement without irradiation of sample should be started as well.
2) Specimen needs to be cleaned as it is described in section 2.1 and mounted into the sample holder. After changing copper gasket of the flange of the sample chamber needs to be closed very tight applying equal force on every screw and purged at least 3 times. Pressure below 10^{-6} mBar should be reached after last purging.

3) Pre-irradiation:
    a) When laser signal is stable chamber is vented to 100 mBar;
    b) 24 h measurement can be started.
4) LIC test
    a) Pumps are shut down and chamber vented to 1000 mBar using ultrapure air.
    b) The chamber is opened under permanent purge with ultrapure air and the contaminant source is placed in the oven intended for contaminant heating.
    c) The flanges of the chamber are shut and the chamber is purged three times with ultrapure air. Afterwards the chamber is evacuated to below 10^{-5} mbar.
    d) To qualify the optical response/behaviour of the set up the vacuum chamber is vented to 100 mBar with ultrapure air and the transmission/fluorescence signal is recorded for about an hour.
    e) To cool down the sample to measurement conditions (T_{sample} = 0 °C) the external cooling system for the Peltier unit needs to be attached. Further the oven temperature for contaminant heating is raised to measurement conditions (ordinary $T_{contaminant}$ = 60 °C).
    f) After temperature equilibration the transmission/fluorescence is recorded at least 72 h (as agreed by Laser development department).

       *If the laser beam energy drop in the transmission arm is more than 15%, measurement can be stopped right away.
5) System behaviour check-up
    a) After stopping the measurement the sample is heated over the dew point chamber to avoid condensation and the measurement chamber is vented to 1000 mBar.
    b) Specimen and contamination source can be taken out.
    c) Chamber is closed and purged 3 times with ultrapure air.
    d) To document the stability of the optical system the measurement chamber is vented to 100 mBar again, and transmission as well as fluorescence is recorded over 1 h.

Vacuum chamber cleaning procedure

1) If there is contamination growth: chamber should be baked-out as described in section 2.3.1.3 and pumped for 72 h or more.
2) If there is no contamination growth: chamber evacuation through the weekend is sufficient to guarantee contamination free operation of the measurement system.

Blank measurement procedure:

1) Blank measurement should be performed for 48 hours (or more) with identical conditions like the LIC test. Blank test ensures that the vacuum chamber is not polluted with organic material from former LIC tests. If during this blank test transmission losses are bigger than 10%, cleaning procedure should be repeated.

3. Results and Discussions

3.1 Optical setup optimization and characterization

Even though the setup described in previous section was used before for similar tests some adjustments of the system were needed. In this section major setup changes and its characterization are discussed. Former LIC tests were performed using toluene gas mixture to see if the setup works and what should be optimized [4], the way the contaminant is introduced to the system had to be changed as contamination sources are in the solid state. For this purpose small oven was installed into the vacuum chamber to accelerate outgassing rate of contamination sources. The possibility to control temperature of the oven not only allows to speed up outgassing of contamination source, but to simulate working environment better as well. It is important for these specific measurements as some of the MOMA laser parts might be of different temperature, which has influence on the outgassing rates. The following optimization steps were necessary to minimize the temperature and optic degradation at 266 nm influence on test results.

3.1.1 Selection of appropriate filters for measurement system

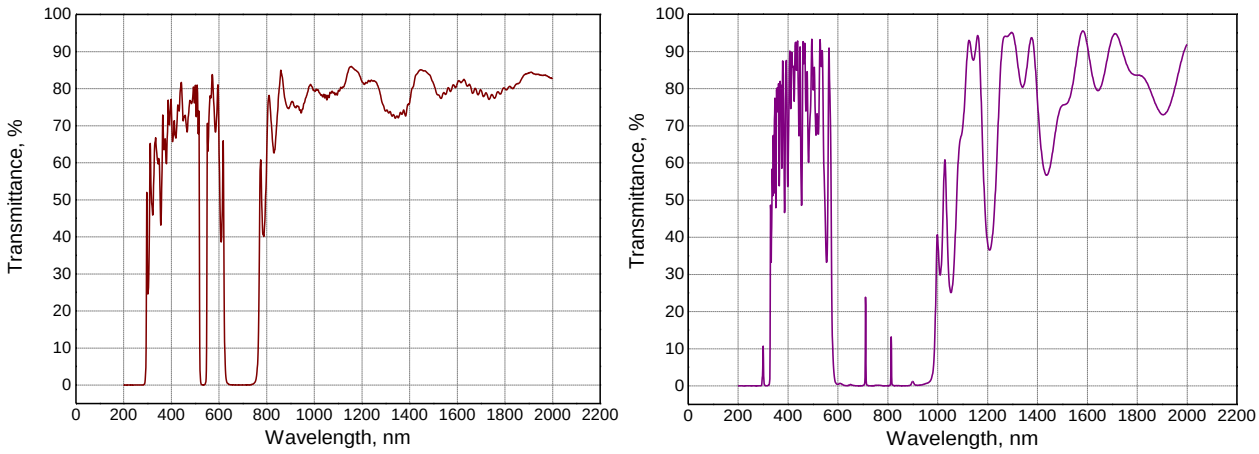

Figure 21. Transmission spectra of filter Nr.1 on the left and filter Nr.2 on the right.

As it was mentioned before, fused silica exposed to 266 nm tends to absorb light due to Non-Bridging Oxygen Hole Centres and Oxygen Deficient Centres. These colour centres emits light at around 610 – 650 nm and 420 nm respectively, and can be mistaken with contamination build-up. To avoid this filter has to be mounted in front of focusing optics of the CMOS camera. Two different filters manufactured in LZH, whose transmission spectra are plotted in Fig. 21, were tried. According to transmission spectra filter Nr. 2 should work better, but as it is seen in Fig. 22 filter Nr. 1 works betters for this application. Even though spot can be seen on the sample (Fig. 22), with additional tests it was confirmed that the intensity of the substrate fluorescence is negligible as the LIF signal is the same in both cases when the sample is and is not exposed to the laser beam.

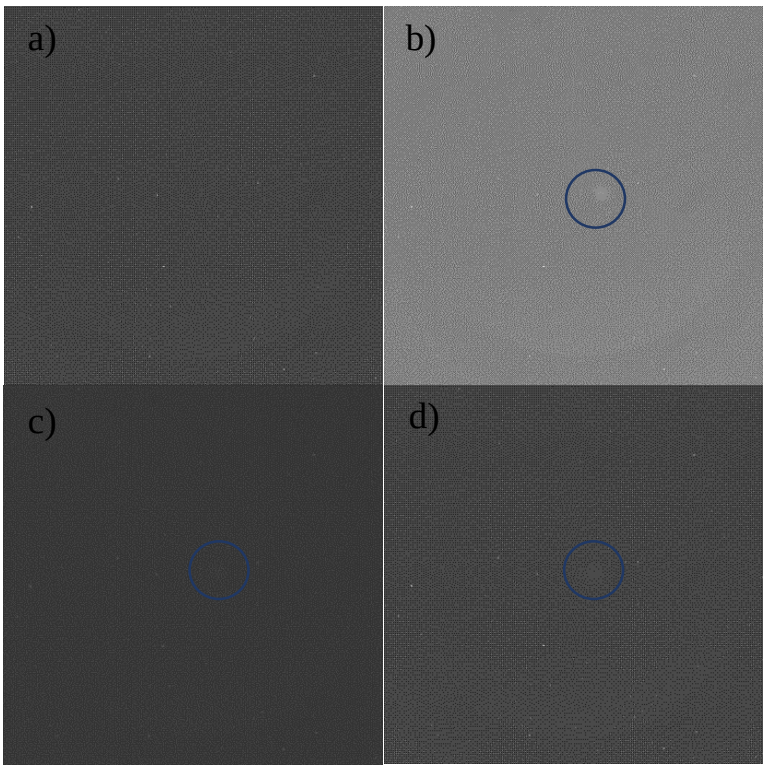

Figure 22. Pictures of a sample plane a) not exposed to the laser beam; irradiated by 266 nm: b) with no filter in front of the camera, c) with filter Nr.1 in front of the camera, d) with filter Nr2. The big circle that is seen close to the edge of pictures is the frame of sample holder. The real height and width are 10 mm.

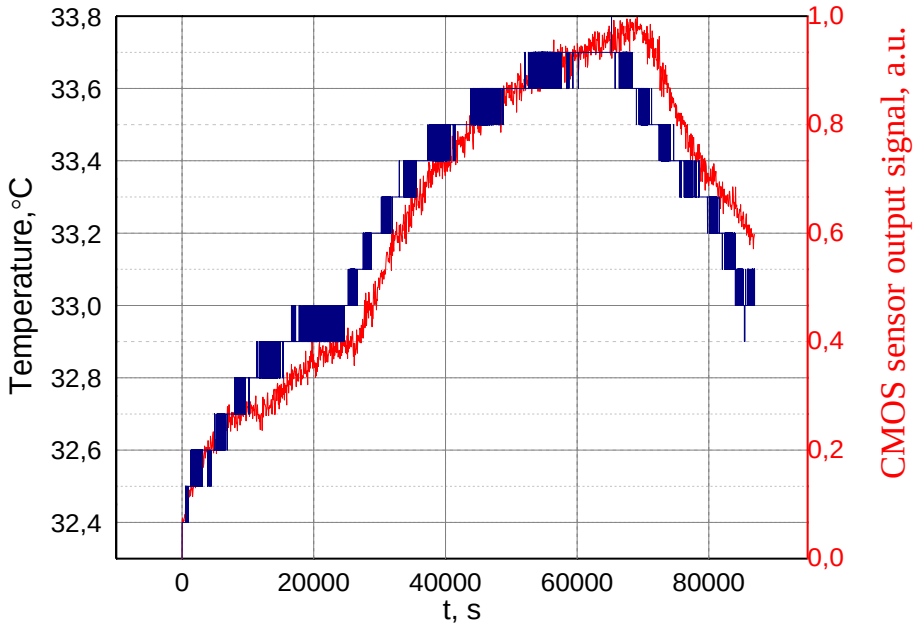

Figure 23. The CMOS sensor output signal (red) and environment temperature profile (blue). The data was collected during LIC measurement, the rise of the signal is not due to laser-induced fluorescence of contamination growth as transmittance monitoring and ex-situ inspection of the sample did not indicate it.

As it can be seen in the Fig. 23, LIF signal or, to be more precise, the output that is generated by the camera is much more sensitive to the temperature change. The CMOS sensor output

voltage increases with temperature as the pixel photocurrent depends on temperature as well as photodiode dark current and noise [47]. This needs to be taken into account while analysing recorded LIF signal of laser-induced contamination measurements.

3.1.2 Effect of temperature on measurement system

Comparing with former LIC tests that were performed using the same optical bench, these LIC measurements have much longer duration. Overnight measurements brought new challenges as many parts of the system appeared to be very sensitive to the temperature change. Additionally, over night temperature changes more than over day, temperature effects might lead to misinterpretation as it influences the recorded signal. To minimize this effect and characterize the influence of temperature following setup changes were done:

1) Pellin Broca prism was mounted instead of HR mirror for directing laser beam and separation of second and fourth harmonics. The laser output ratio of second and fourth harmonics slightly changes with the temperature, but it would be enough to bring big deviations in measured signal power. Even though there is just small amount of SH coming out of the laser, photodiodes appeared to be very sensitive for this wavelength: the responsivity of the used photodiodes is approximately one order of magnitude higher for 532 nm wavelength than for 266 nm. Even small portion of residue 532 in the laser beam influences the transmission signal. Filtering out SH and without changing anything else the signal of photodiodes decreased around 3 and 2,5 times in reference and transmission arms respectively.
2) Few different setups for coupling out portion of laser beam was tried: two nearly parallel substrates, HR mirror and AR coated substrate. Parallel optical surfaces create etalon, its distance strongly depends on the temperature. Consequently, it has big influence on interference of the waves and signal. Using AR coated substrate for coupling out portion of the laser beam seems to be the least sensitive to temperature changes.
3) Laser output power (wavelength 266 nm) strongly depends on its temperature due to non-temperature controlled nonlinear crystals. As it can be seen in the Fig. 24 at the temperature range from 25,8 to 32,5 °C laser output power drops by 40%. Constant temperature and therefore laser output power are reached using external heater. While measuring laser output power dependence on its temperature, the beam profile was checked constantly as well. In the same temperature range the major width of the beam got reduced by 11% while minor width – 6%. This implies that beam profile should be measured after reaching stable laser temperature, which is 33 °C for this specific system.
4) Temperature in the laboratory was stabilized as well.

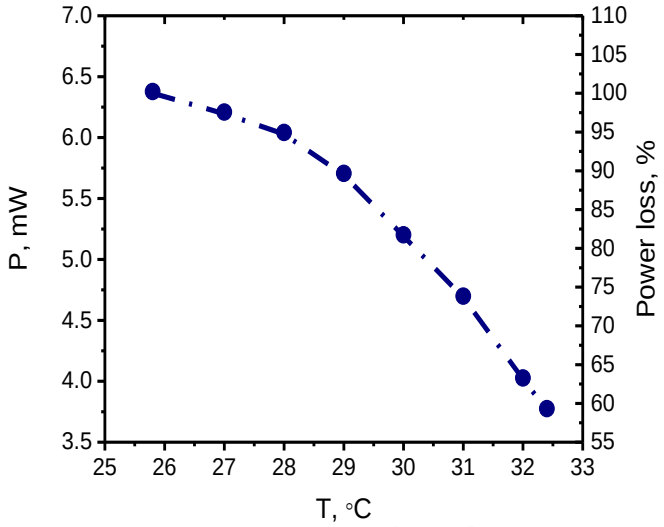

Figure 24. Laser output power dependence on its temperature.

3.1.3 Transmission signal baseline correction

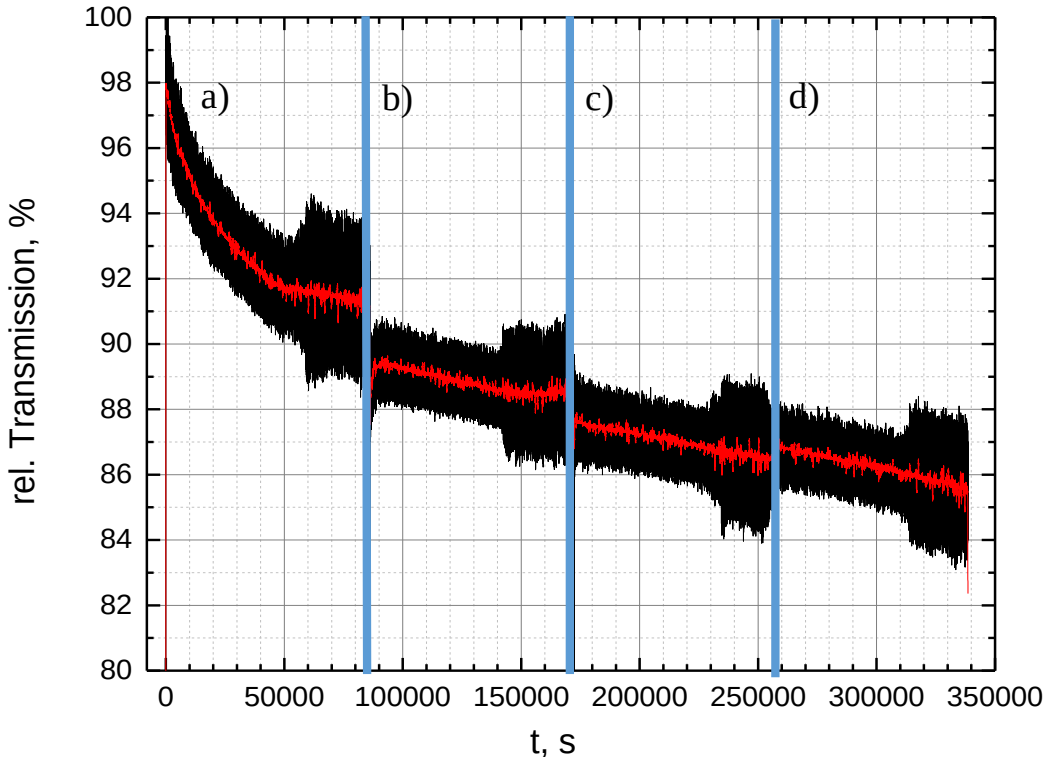

Figure 25. LIC setup referenced (normalized) transmission signal (black) behaviour through the time: a) laser beam entrance and exit windows are taken out as well as the sample is not placed, b) vacuum chamber windows are placed, c) optical sample is mounted in the sample holder, d) new optical sample is placed. Red line is averaged transmission signal. Measurement is done in ambient conditions.

With all the adjustments mentioned above constant referenced transmission signal – the ratio of laser beam power in reference and transmission arms – was not reached. As there were no signs of possible contamination build-up, the decrease in transmission signal could mean degradation in optical components due to exposure to UV radiation as well as desorption of adsorbed water on

optical surfaces. It was decided to record baseline that represents behaviour of optical setup as it was noticed that during every long-term measurement system undergoes typical transmission losses. LIC setup relative transmission signal recorded in 4 steps is plotted in Fig. 25. This plot is very important for data analysis. First 24 hour measurement (step a) was done without specimen and chamber windows. The optics, which is placed behind the shutter degrades around 7% in this time of period (exponential decay). Second measurement (step b) was performed after setting in both chamber windows. At first, signal was rising due to surface cleaning effect, afterword signal decreased around 1% in 24 h (linear decay). Steps c and d were done with optical samples. Signal decreases around 0,5% as AR coated substrate transmission is 99,6%. With optical sample inside the chamber signal decreases around 1,5% in 24h. As difference between steps c and d is equal 0,5% and the rest of optical components of transmission arm cause transmission losses of ~ 1% in 24 h (step b), it is safe to conclude that sample degradation in 24 h is equal 0,5%. During measurement lasting 96 h, relative transmission signal decrease by 12 – 13% is expected. Although to evaluate system behaviour more precisely, measurement performed under real tests conditions (zero measurement) is needed.

3.1.4 Zero measurement

First zero measurement was done with all the steps described in 2.3.2 section besides contamination source introduction to the system. According to this measurement that is plotted in Fig. 27 data of LIC tests will be analysed. Additionally, zero measurement is needed to ensure that vacuum chamber is clean and there will be no cross contamination. DIC micrograph of zero measurement sample is plotted in Fig. 26. a), there is no contamination build-up during LIC test. For comparison, DIC micrograph of contaminated sample is plotted in Fig. 26. b). Contamination source – toluene, pressure $8*10^{-6}$ mBar, λ = 266 nm. During measurements with toluene gas that were already mentioned before, the vacuum chamber was strongly contaminated and it took long time till it was properly cleaned.

Laser-induced fluorescence signal is not constant (Fig. 27), but as transmission signal dropped around 7% in 96 hours, which is a less than expected due to optics degradation, these oscillations are probably due to temperature change in the laboratory. Additionally, there was no contaminant source in the chamber so there should not be any contamination build-up. When the specimen is out and the environment of the test is restored, signal is around 2% higher. As it is seen in the Fig. 25, this is how much optical sample is expected to degrade in 96 h. In the real LIC tests when signal rise is 2-3% in the last step of the measurement it will be assumed that there was no contamination build-up during measurement. Additionally, offline DIC microscopy inspection does not show any signs of contamination build-up.

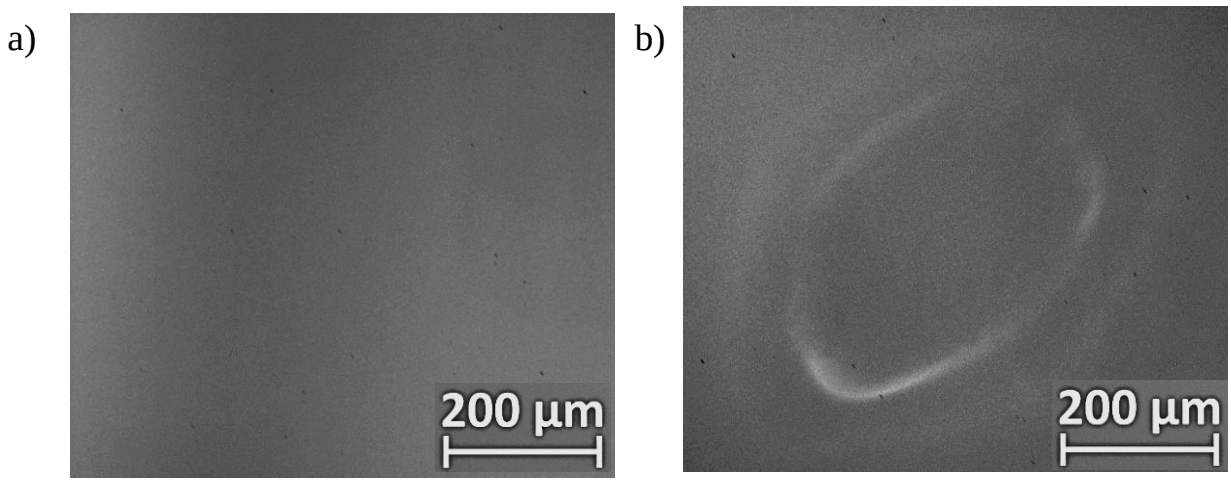

Figure 26. DIC micrographs of a) successful zero measurement – no deposit formation, b) laser-induced contamination deposit that built-up during first zero measurement done after LIC tests with toluene. Deposit resembles donut shape, the smaller circle is the peak of it and bigger circle – the edge of the contaminant growth.

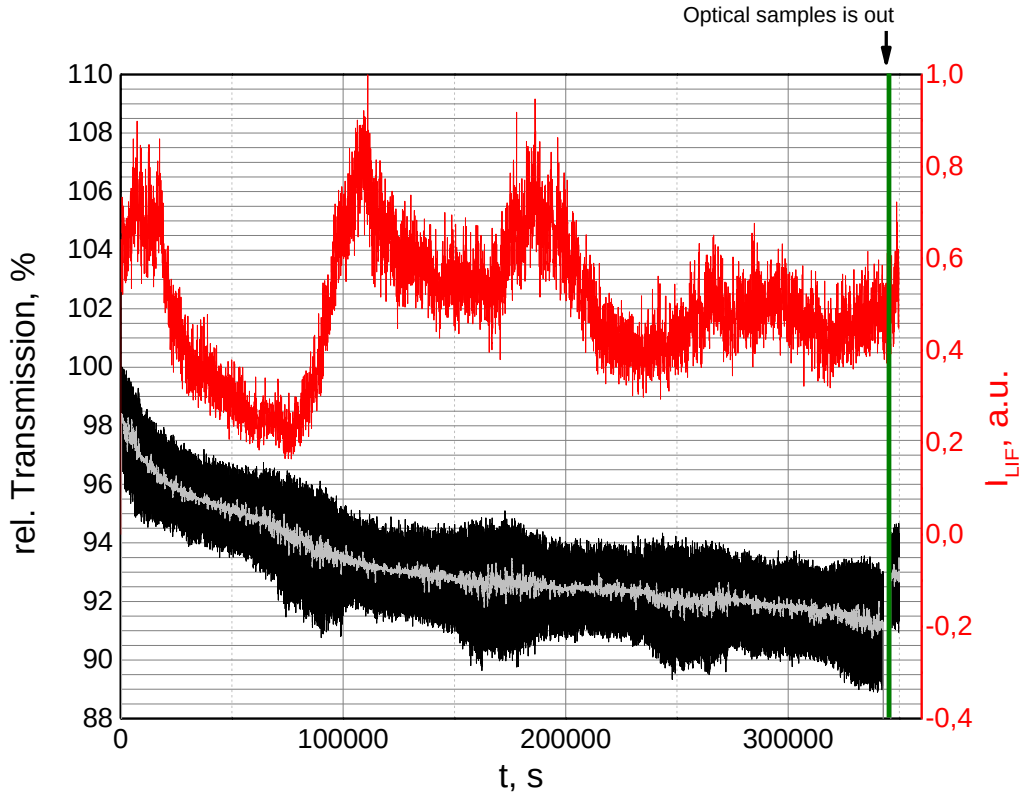

Figure 27. Zero measurement. Red line – LIF signal, black – transmission signal, grey – averaged transmission signal.

3.2 LIC investigations

3.2.1 Epoxy “Loctite Ablestik 2151” investigation: contamination growth on anti-reflective coating

The outgassing of epoxy can be suppressed by proper preparation and bake-out. As there is no information on how this epoxy should be baked-out not to cause LIC on optics irradiated by

266 nm, epoxy was baked-out for 24 h. If there is contamination, new preparation procedure should be applied or other kind of epoxy chosen.

As it can be seen in Fig. 28, transmission signal after 96 hours of irradiation (3500000 pulses) decreased by 8,5%, that is around 4 % less than expected signal drop due to optics degradation. Comparing it to zero measurement (Fig. 30), relative transmission in the end of measurement is around 1,5% smaller, although during pre-irradiation step (no contamination source inserted) signal decreased for ~1,5%, most likely this difference is not due to contamination growth. When the specimen is out, signal is only 3% higher. LIF signal rose the most while sample was not irradiated, meaning that it is due to heating of the camera and comparing with temperature curve it is seen that LIF signal oscillations are due to temperature change. Ex-situ investigation does not show any signs of contamination build-up. Taking into account Zero measurement, this allows to assume that there is no LIC growth or it is too small to detect it. Epoxy, prepared in this way, is compatible for MOMA laser. After measurement chamber was cleaned and blank test performer to ensure that there would be no cross contamination.

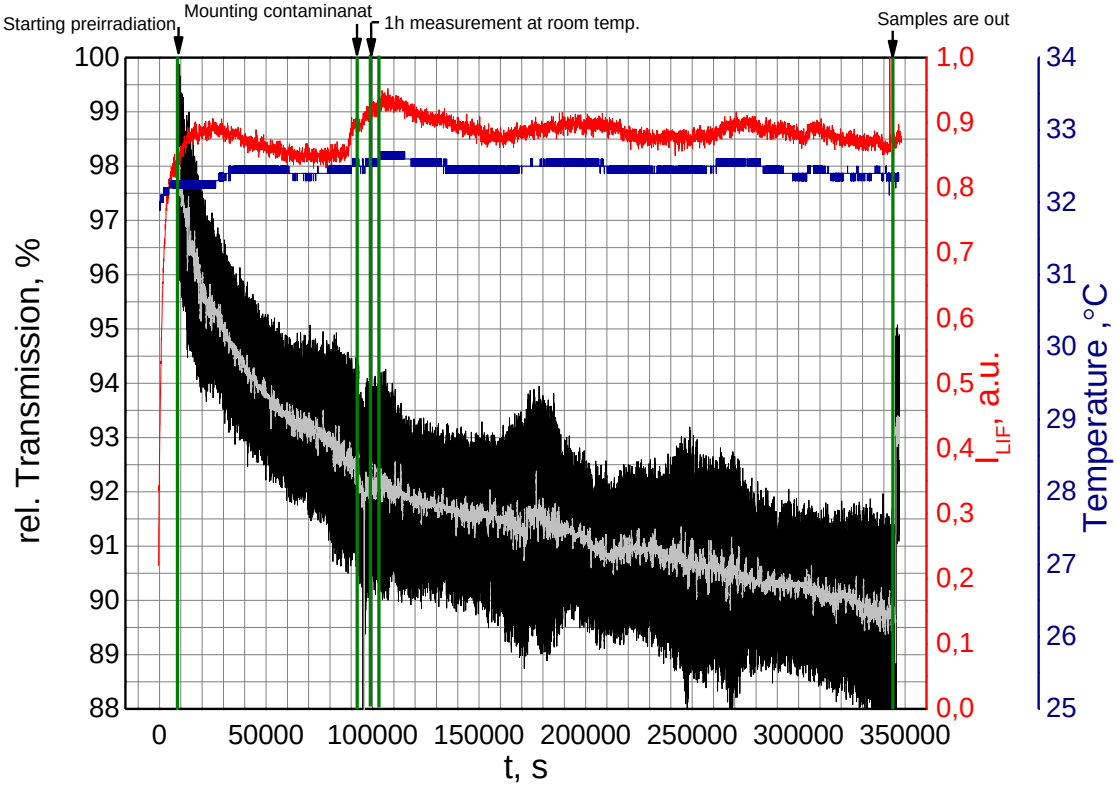

Figure 28. Laser-induced contamination 96 h measurement. Contamination source: epoxy "Loctite Ablestik 2151". Red line – LIF signal, black – transmission signal, grey – averaged transmission signal, blue – laser temperature.

3.2.2 Investigation of electrical plugs: contamination growth on anti-reflective coating

Transmission signal after 96 hours of irradiation (3,5 million (mln.) pulses) decreased by 8%, that is around 5% less than expected signal drop due to optics degradation. When the specimen

is out, signal is only 2% higher. During time intervals where no transmission signal is registered either sample was being mounted or taken out. During the measurements there was immediate decrease of transmission signal at around 100000 s, and then signal increased back. It was chosen to ignore this part as if there is contamination growth, transmission signal decreases gradually, and even when cleaning process takes place, transmission signal does not reach its initial value and it is not this rapid either. Most likely some object got into beam path and cut part of it. LIF signal rose the most while sample was not irradiated, meaning it is due to camera's heating and most oscillations are due to temperature change. LIF signal reached its maximum value at around 350000 s cause vacuum chamber was opened and external light entered the chamber. Ex-situ investigation does not show any signs of contamination build-up. Taking into account Zero measurement (Fig. 27), this allows to assume that there is no LIC or it is negligible. Electrical plugs are compatible for MOMA laser.

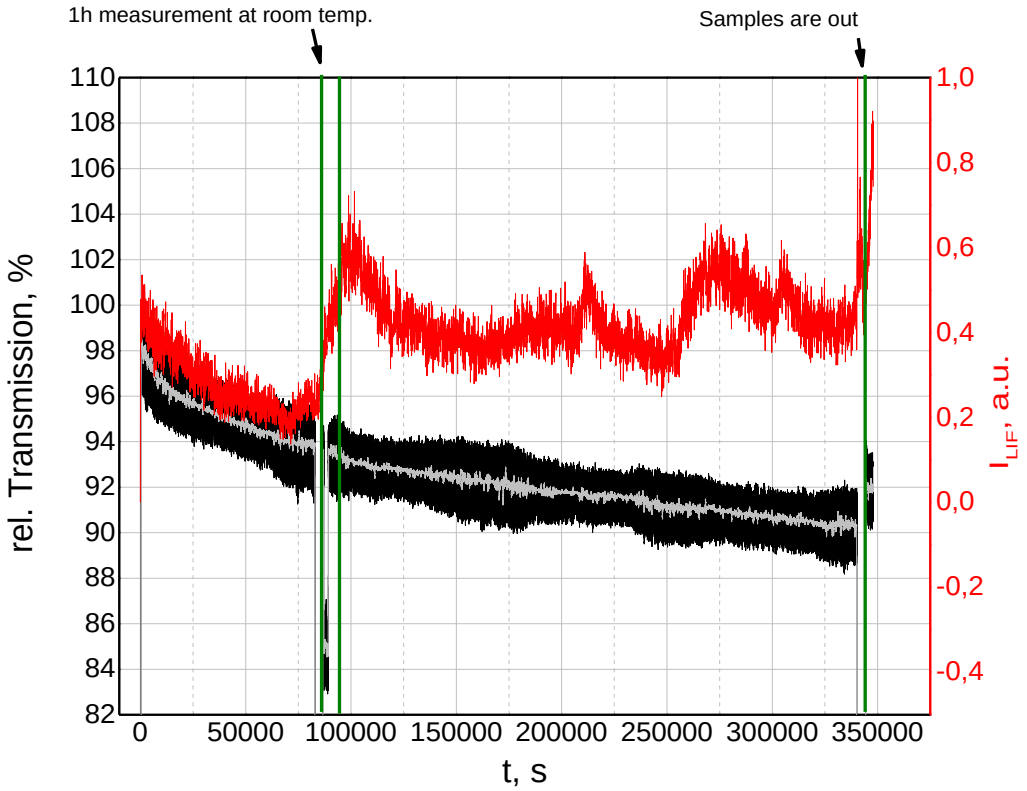

Figure 29. Laser-induced contamination 96 h measurement. Contamination source: electrical plugs. Red line – LIF signal, black – transmission signal, grey – averaged transmission signal.

3.2.3 Comparison of transmission loss during zero and LIC measurements

Comparison of averaged relative transmission during zero and LIC tests is plotted in Fig. 30. Clearly, rel. transmission after 96 h measurement differ during all the tests, but only by 0,5 – 1%. This result is acceptable as the optical components when exposed to the 266 nm radiation always degrade slightly in a different manner.

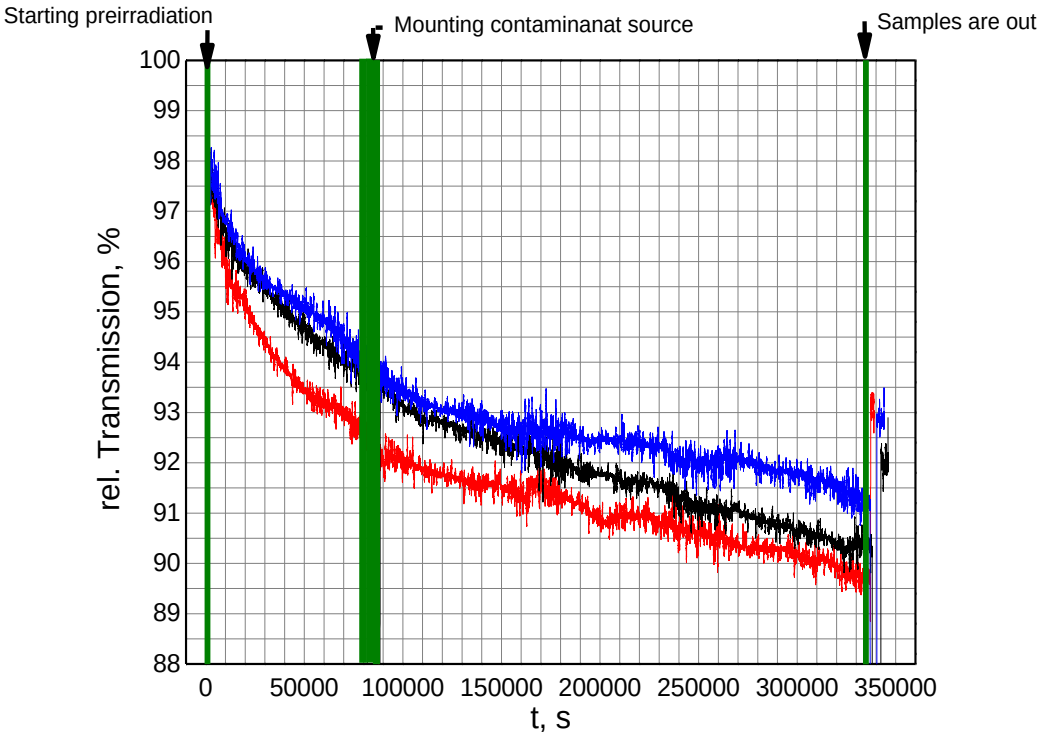

Figure 30. Averaged relative transmission during zero measurement (blue), LIC test with "Loctite Ablestik 2151" (red) and electrical conectors (black).

4. Conclusions

1) Dedicated optical setup with two in-situ monitoring methods and ex-situ investigation was assembled and can be used for long term laser-induced contamination measurements, nevertheless careful consideration of specific measurement procedure involving appropriate characterization of the test bench is required to avoid possible misinterpretation of laser-induced contamination data, especially Laser-Induced Fluorescence signal, due to high influence of temperature changes and optics degradation under 266 nm radiation exposure.

2) After approximately 2,6 mln. laser pulses (72 hours), epoxy “Loctite Ablestik 2151” and the alternative electrical plugs do not cause measurable laser-induced contamination growth on tested optics under simulated working conditions. There were neither noticeable transmission loss nor sufficient rise in Laser-Induced Fluorescence signal nor visible deposit under inspection with Nomarski microscope. It is a good candidate for use in Mars Organic Molecule Analyser laser system.

3) Synthetic air that is used to pressurize Mars Organic Molecule Analyser’s laser compartment for reduction of LIC effect is good candidate mitigating formation of deposit as during performed 72 hour worst case scenario tests with possible contamination sources, there were no significant signs of contamination growth. Comparative LIC measurements different kind of gas mixture and vacuum environments are needed to confirm the mitigation effect.

Literature

[1] The ExoMars Rover Instrument Suite: MOMA - Mars Organic Molecule Analyzer, European Space Agency, [Online]. Available: http://exploration.esa.int/mars/45103-rover-instruments/?fbodylongid=2132. [Accessed 29 04 2016].

[2] C. Kolleck, A. Büttner, M. Ernst, M. Hunnekuhl, T. Hülsenbusch, A. Moalem, M. Priehs, D. Kracht and J. Neumann, Enhancement of the Design of a Pulsed UV Laser System for a Laser-Desorption Mass Spectrometer on Mars, in: *International Conference on Space Optics (ICSO)* (2012).

[3] W. Brinckerhoff, V. Pinnick, F. van Amerom, R. Danell, R. Arevalo, M. Atanassova, X. Li, P. Mahaffy and R. Cotter, Mars Organic Molecule Analyzer (MOMA) Mass Spectrometer for ExoMars 2018 and Beyond, in: *44th Lunar and Planetary Science Conference* (2013).

[4] M. Ließmann, L. Jensen, I. Balasa, M. Hunnekuhl, A. Büttner, P. Weßels, J. Neumann and D. Ristau, Scaling of Laser-induced Contamination Growth at 266 nm and 355 nm, Proc. of SPIE: Laser-Induced Damage in Optical Materials, vol. 9632 (2015).

[5] D. Wernham, Optical Coatings in Space, Proc. of SPIE: Advances in Optical Thin Films, vol. 8168 (2011).

[6] L. Jensen, M. Jupé, H. Mädebacha, H. Ehlersa, K. Starke, D. Ristau, W. Riede, P. Allenspacher and H. Schroeder, Damage Threshold Investigations of High Power Laser Optics under Atmospheric and Vacuum Conditions, Proc. of SPIE: Laser-Induced Damage in Optical Materials, vol. 6403 (2006).

[7] K. Mikami, S. Motokoshib, M. Fujitab, T. Jitsunoa and K. Tanaka, Laser-Induced Damage Thresholds of Optical Coatings at Different Temperature, Proc. of SPIE: Laser-Induced Damage in Optical Materials, vol. 8190 (2011).

[8] K. Mikami, S. Motokoshi, T. Somekawa, T. Jitsuno, M. Fujita and K. Tanaka, Temperature Dependence of Laser-Induced Damage Threshold of Optical Coatings at Different Pulse Widths, Optics Express, vol. 21 (2013).

[9] M. Otta, D. Coylea, J. S. Canham and H. W. Leidecker, Qualification and Issues with Space Flight Laser Systems and Components, Proc. SPIE: Solid State Lasers XV: Technology and Devices, vol. 6100 (2006).

[10] D. Wernham, J. Alves, F. Pettazzi and A. Tighe, Laser-Induced Contamination Mitigation on the ALADIN Laser for ADM-Aeolus, Proc. of SPIE: Laser-Induced Damage in Optical Materials, vol. 7842 (2010).

[11] David Catling, Atmospheric Evolutions of Mars, in: *Encyclopedia of Paleoclimatology and Ancient Environments*, V. Gornitz, Ed. (Springer, 2008) pp. 66-75.

[12] R. M. Haberle, Mars: Atmosphere, in: *Encyclopedia of Planetary Sciences*, Shirley, Ed. (Springer, 2000) pp. 432-441.

[13] W. Riede, H. Schröder, D. Wernham and A. Tighe, UV Laser-Induced Hydrocarbon Contamination on Space Optics, in: *SRI Satellite Workshop: Carbon Contamination of Optics* (2012).

[14] A. Tighea, F. Pettazzib, J. Alves, D. Wernham, W. Riede, H. Schroederd, P. Allenspacherd and H. Kheyrandish, Growth Mechanisms for Laser-Induced Contamination on Space Optics in Vacuum, Proc. of SPIE: Laser-Induced Damage in Optical Materials, vol. 7132 (2008).

[15] A. Pereira , J.-F. Roussel, M. V. Eesbeek, J. Guyt, O. Schmeitzky and D. Faye, Study of the UV-Enhancement of Contamination, Proceedings of the 9th International Symposium on Materials in a Space Environment (2003).

[16] H. Schroder, W. Riede, H. Kheyrandish, D. Wernham and Y. Lien, Investigation of UV Laser Induced Depositions on Optics under Space Conditions in Presence of Outgassing Materials, in: *Proceedings of ESA/CNES ICSO, sixth International Conference on Space Optics* (2006).

[17] H. Schröder, W. Riede, E. Reinholdb, D. Wernhamb, Y. Lien and H. Kheyrandishc, In Situ Observation of UV Laser-Induced Deposit Formation by Fluorescence Measurement, Proc. of SPIE: Laser-Induced Damage in Optical Materials, vol. 6403 (2006).

[18] A. Pereira, E. Quesnel and M. Reymermier, Dynamic Measurements of Ultraviolet-Enhanced Silica Contamination by Photoluminescence-Based Diagnostic, Journal of Applied Physics (2009).

[19] H. A. Abdeldayem, E. Dowdye and J. Canham, Roles of Contamination and Nonlinear Effects in Failing Space-Flight Lasers, Applied Physics B, Lasers and Optics, 447–452 (2006).

[20] H. A. Abdeldayem, E. Dowdye, J. Canham and T. Jaeger, Contamination and Radiation Effects on Spaceflight Laser Systems, Photonics for Space Environments X, Proceedings of SPIE, vol. 5897 (2005).

[21] D. J. S. Canham, Investigation of Contamination Effects on Laser Induced Optical Damage in Space Flight Lasers, [Online]. Available: https://esto.nasa.gov/2012test/conferences/estc2004/papers/b2p2.pdf. [Accessed 25 04 2016].

[22] J. Scialdone, Pressure and Purging Effects on Material Outgassing and Evaporation, Proceedings of the 9th International Symposium on Materials in a Space Environment, 203-207, 2003.

[23] H. Schröeder, P. Wagner, D. Kokkinos, W. Riede and A. Tighe, Laser-Induced Contamination and its Impact on Laser Damage Threshold, Proc. of SPIE: Laser-Induced Damage in Optical Materials, vol. 8885 (2013).

[24] J. Alves, F. Pettazzi, A. Tighe and D. Wernham, Laser-Induced Contamination Control for High-Power Lasers in Space-Based Lidar Missions, in: *International Conference Space Optics – ISCO* (Rhodes, Greece, 2010).

[25] W. Riede, H. Schröeder, G. Bataviciute, D. Wernham, A. Tighe, F. Pettazzi and J. Alves, Laser-Induced Contamination on Space Optics, Proc. of SPIE: Laser-Induced Damage in Optical Materials, vol. 8190 (2011).

[26] J. S. Canham, Molecular Contamination Damage Prevention Lessons Learned from Vacuum Laser Operation, Proc. of SPIE: Laser-Induced Damage in Optical Materials, vol. 5991 (2005).

[27] D. Nguyen, L. Emmert, W. Rudolph, D. Patel, E. Krous, C. Menoni and M. Shinn, Studies of Femtosecond Laser Induced Damage of HfO2 Thin Film in Atmospheric and Vacuum Conditions, Proc. of SPIE: Laser-Induced Damage in Optical Materials, vol. 7504 (2009).

[28] P. Wagner, Laser-Induced Contamination on High-Reflective Optics, D. H. S. Prof. Dr. Wolfgang Heddrich, Ed. (University of Applied Science Darmstadt, DLR - German Aerospace Center, Germany, 2014).

[29] Magnetron Sputtering Technology, Micro Magnetics, Inc., [Online]. Available: http://www.directvacuum.com/pdf/what_is_sputtering.pdf. [Accessed 25 04 2016].

[30] J. Böhlmark , Fundamentals of High Power Impulse Magnetron Sputtering (Linköping University, Institute of Technology, Sweden, 2005).

[31] D. Christie, Making Magnetron Sputtering Work: Reversing the Glow to Arc Transition, Advanced Energy Industries, Inc., Fort Collins, CO, 2014. [Online]. Available: http://www.advanced-energy.com/upload/file/reprints/2014_spring_dchristie_pp32-36.pdf. [Accessed 25 04 2016].

[32] T. Turner and R. Kirschner, Photonics Handbook of Thin-Film Coatings: A Buyers' Guide, Research Electro-Optics, Inc. (REO), [Online]. Available: http://www.photonics.com/EDU/Handbook.aspx?AID=42399. [Accessed 20 04 2016].

[33] Farotex: A Brief Explanation of How Magnetron Sputtering Works, [Online]. Available: http://farotex.com/technology.html. [Accessed 25 04 2016].

[34] Module 6-5: Mirrors and Etalons, [Online]. Available: http://pe2bz.philpem.me.uk/Lights/-%20Laser/Info-902-LaserCourse/c06-05/mod06_05.htm. [Accessed 24 04 2016].

[35] P. Misra and . M. A. Dubinskii, Ultraviolet and Vacuum Ultraviolet Sources and Materials for Lithography, in: *Ultraviolet Spectroscopy And UV Lasers* (Marcel Dekker Inc., New York, 2002) pp. 1-32.

[36] R. Salh, Defect Related Luminescence in Silicon Dioxide Network: A Review, in: *Crystalline Silicon – Properties and Uses*, P. S. Basu, Ed. (InTech, 2011) pp. 135-172.

[37] M. Cannas and F. Messina, Nd:YAG Laser Induced E' Centers Probed by In-Situ Absorption Measurements, Journal of Non-Crystalline Solids, vol. 351, 1780–1783 (2005).

[38] F. Messina and M. Cannas, Stability of E' Centers Induced by 4.7eV Laser Radiation in SiO2, Journal of Non-Crystalline Solids , vol. 353, 522-525 (2007).

[39] M. Beresna, M. Gecevičius and P. G. Kazansky, Ultrafast Laser Direct Writing and Nanostructuring in Transparent Materials, Advances in Optics and Photonics, vol. 6 (2014).

[40] S. Girard, J. Kuhnhenn, A. Gusarov, B. Brichard , M. V. Uffel, Y. Ouerdane, A. Boukenter and C. Marcandella, Radiation Effects on Silica-Based Optical Fibers: Recent Advances and Future Challenges, IEEE: Transactions on Nuclear Science, vol. 60 (2013).

[41] Uncoated UV-Grade Fused Silica, [Online]. Available: https://www.thorlabs.com/newgrouppage9.cfm?objectgroup_id=6973&tabname=UV%20Fused%20Silica. [Accessed 18 05 2016].

[42] S. Borgmann, W. Riede, D. Wernham and H. Schroeder, Investigation of Laser-Induced Deposit Formation under Space Conditions, in: *International Conference on Space Optics* (Toulouse, 2008).

[43] H. Schröder, S. Becker, Y. Lien, W. Riede and D. Wernham, Fluorescence Monitoring of Organic Deposits, Proc. of SPIE: Laser-Induced Damage in Optical Materials, vol. 6720 (2007).

[44] Molecular Expressions, [Online]. Available: https://micro.magnet.fsu.edu/primer/techniques/dic/dicoverview.html. [Accessed 26 04 2016].

[45] R. J. Oldfield, Differential Interference Contrast Light Microscopy, Encyclopedia of Life Sciences (2001).

[46] Outgassing Data for Selecting Spacecraft Materials, [Online]. Available: https://outgassing.nasa.gov/. [Accessed 27 04 2016].

[47] H. Zimouche, H. Amhaz and G. Sicard, Temperature Compensation Scheme for Logarithmic CMOS Image Sensor, International Image Sensor Workshop, IEEE Computer Society,138-141 (2011).

Summary

New ExoMars rover mission led by ESA will launch on 2018 with the aim of seeking for the manifestations of life. For molecular compound characterization ExoMars rover contains Mars Organic Molecule Analyser (MOMA). To ensure efficient sample preparation nanosecond-pulsed frequency-quadrupled (266 nm) passively Q-switched Nd:YAG laser with the intensities of tens to hundreds of Mega Watts in squared centimetre (MW/cm^2) is used. Development of high-power laser systems for space applications is not straightforward, analysis of previously failed space missions showed that the lifetime of ultraviolet laser optics in space is lowered due to the vacuum impact on material outgassing rates and laser-induced contamination (LIC). The development of MOMA laser-system and for the qualification of used optical components and materials regarding LIC are entrusted to The Laser Zentrum Hannover e.V.

Monitoring of laser-induced contamination growth under near-operation MOMA environmental conditions on AR-coated substrates was performed using two in-situ and one ex-situ investigation methods. Two possible MOMA laser-system contamination sources were tested: epoxy "Loctite Ablestik 2151" and electrical plugs that might contain small amount of organic compounds. After approximately 2,6 mln. laser pulses (72 hours), neither of contaminants cause measurable laser-induced contamination growth on optics exposed to 266 nm wavelength, it is confirmed by complementary investigation units. Synthetic air containing oxygen (O_2) is used to pressurize Mars Organic Molecule Analyser's laser compartment for reduction of LIC effect. O_2 is known as mitigating LIC factor and plausibly even under 100 mBar pressure oxygen content is sufficient to supress contamination growth. Comparative LIC measurements in different kind of gas mixture and vacuum environments are needed to confirm the mitigation effect.

Santrauka

Lazerinių technologijų vystymasis atveria duris į naujas panaudojimo sritis. Vis daugiau lazerinių sistemų yra įmontuojama erdvėlaiviuose kosminiams tyrimams. Tačiau, iki šiol susiduriama su daug praktinių sunkumų susijusių su itin aršia kosmoso aplinka, kuri sąlygoja įvairius optinių elementų savybių pakitimus, tokius kaip pažaidos lazerio spinduliuote slenksčio mažėjimas ir lazerinės spinduliuotės sugerties didėjimas. 2018 m. ExoMars antrosios misijos metu ant Marso paviršiaus bus nuleistas marsaeigis. Šios misijos metu bus ieškoma gyvybės pėdsakų Marse. Marsaegyje įmontuotas Marso Organinių Molekulių Analizatorius (MOMA), kuriame molekulinių junginių charakterizavimui naudojamas masės spektrometras, o bandinių paruošimui – Nd:YAG lazerio ketvirtoji harmonika. 266 nm bangos ilgio spinduliuotės intensyvumas siekiantis dešimtis-šimtus MW/cm2 užtikrina efektyvią molekulių nuo Marso paviršiaus desorbciją ir jų jonizaciją. Tai yra pirmoji kosminė misija naudojanti lazerį, kurio bangos ilgis 266 nm, todėl iki šiol praktiškai nėra informacijos apie kosmoso aplinkos įtaką optinių elementų, apšviestų 266 nm bangos ilgio spinduliuote, savybėms. Vakuume patalpintos organinės medžiagos yra linkusios garuoti greičiau negu įprastomis sąlygomis. Šios atitrūkusios molekulės yra pritraukiamos didelio intensyvumo spinduliuote, prispaudžiamos prie optinių paviršių, kur ir suformuoja molekulinius darininius – tai vadinama lazerine spinduliuote sukelta tarša (LSST). Dėl šios taršos sumažėja optinių elementų pralaidumas ir pažaidos lazerio spinduliuote slenkstis, ir tai sąlygoja kosminės misijos gyvenimo trukmės sumažėjimo grėsmę. Ultravioletinė spinduliuotė paskatina monomerų polimerizaciją, bei yra sugeriama daugelio organinių junginių, dėl to netinkamai parinkus lazerinės sistemos medžiagas yra didelė LSST tikimybė. Norint išvengti misijos sustabdymo dėl optinių elementų netinkamo funkcionavimo, yra svarbu ištirti jų veikimą darbinėse sąlygose ir sumažinti kiek įmanomą LSST sukeliančių faktorių. MOMA lazerinės sistemos vystymas ir optinių elementų, bei medžiagų galinčių sukelti taršą kvalifikavimas yra patikėtas Hanoverio Lazerių Centrui, Vokietija.

Darbo tikslas: įvertinti galimą lazerinės spinduliuotės sukeltą taršą ant Marso Organinių Molekulių Analizatoriui skirtos skaidrinančios dangos.

Matavimams buvo naudojamas stendas skirtas LSST matavimams su 355 nm bangos ilgio spinduliuote. Stendas buvo pritaikytas ketvirtosios Nd:YAG harmonikos ilgalaikiams matavimams pakeitus optinius elementus bei stabilizavus lazerio ir aplinkos temperatūrą. Lazerine spinduliuote sukeltos taršos augimas buvo stebimas matuojant santykinį pralaidumą, lazerio spinduliuote sukeltą fluorescenciją ir taip pat tikrinant bandinį Nomarski tipo mikroskopu po atliktų tyrimų. Kadangi naudojama UV spinduliuotė yra didelė tikimybė, kad susikaupę organiniai dariniai ant optinio paviršiaus turės sugerties juostas šioje bangų srityje. Tokiu būdu santykis tarp spinduliuotės energijos prieš optinį elementą ir už jo mažės taršai didėjant. Organiniai dariniai

kaupiasi tik toje srityje, kur optinis paviršius yra apšviestas lazerine spinduliuote ir energijos tankis yra pakankamai didelis. Molekulės sugerdamos lazerinę spinduliuotę yra sužadinamos ir spinduliuoja šviesą regimąjame diapozone, todėl matavimų metu yra stebima fluorescencija.

LSST matavimai buvo atlikti su dviem galimais MOMA lazerinės sistemos taršos šaltiniais: epoksidiniais klijais “Loctite Ablestik 2151” ir atsarginiais elektros kištukais (3 vnt.), kuriuose naudojami mažai garuojantys epoksidiniai klijai (šių klijų informacija įslaptinta). Abu bandiniai buvo kaitinami vakuuminėse krosnyse 24 valandas, toks bandinių paruošimas turėtų sumažinti medžiagų garavimą vakuume. LSST matavimų metu buvo sukurtos sąlygos artimos MOMA lazerio darbinėms: 100 milibarų atmosfera sukurta naudojant sintetinį orą (79% – azoto, 20% – deguonies ir 1% helio), bandinio laikiklis buvo atšaldomas iki 0 °C, o taršos šaltiniai kaitinami iki 60 °C temperatūros.

Visi trys LSST stebėjimo metodai patvirtina, kad per 72 val. (t.y. po 2,6 milijonų impulsų) tyrimų metu nebuvo užregistruotas taršos augimas. Tai reiškia, kad epoksidinių klijų “Loctite Ablestik 2151” ir elektronių kištukų paruošimo būdas yra tinkamas ir gali būti naudojami MOMA lazerio sistemoje. Bet vis dėlto, matavimai buvo trumpesni negu numatyta misijos gyvenimo trukmė ir norint įsitikinti, kad šie elementai tikrai nesukels taršos reikia atlikti ilgalaikius, misijos gyvenimo trukmę atitinkančius matavimus. Ankstesnių tyrimų metu buvo pastebėta, kad pakankama deguonies koncentracija aplinkoje sumažina lazerine spinduliuote sukeltos taršos augimą ir tai gali būti gautų rezultatų priežąstis. Norint patikrinti ar ištikrųjų sintetinis oras slopina LSST susidarymą reikia atlikti analogiškus tyrimus vakuume ir ore.